

# Aerostructural Optimization and Comparative Study of Twin-Fuselage and Strut-Braced-Wing Aircraft Configurations\*

Yiyuan Ma\*, Morteza Abouhamzeh†

*Technische Universität Braunschweig, Braunschweig, 38108, Germany*

and

Ali Elham‡

*University of Southampton, Southampton SO16 7QF, United Kingdom*

The Ultra-High Aspect Ratio Wing (UHARW) concept is a promising configuration to achieve future sustainable aviation goals. Twin-Fuselage (TF) and Strut-Braced-Wing (SBW) configurations are characterized by smaller structural bending moments and shear forces in the wing and are promising concepts for realizing UHARW designs. This paper addresses the aerostructural optimization problem of TF and SBW configurations with UHARW by using a coupled adjoint aerostructural optimization tool, which is composed of a geometrically nonlinear structural solver and a quasi-three-dimensional Natural Laminar Flow (NLF) aerodynamic solver. The optimization results show significant improvements in fuel efficiency and performance for the TF and SBW aircraft, with fuel mass reduction of 13% and 10%, respectively, compared to the corresponding baseline aircraft designed in the conceptual design phase. In comparison to the original reference aircraft A320neo, the optimized TF and SBW have 48% and 31% lower fuel weight, respectively. The NLF range of both upper and lower wing surfaces is expanded during the optimization. The optimized SBW configuration has a wing aspect ratio of 26.01, while the optimized TF has a wing aspect ratio of 20.74, indicating that the SBW concept is more conducive to realizing UHARW design compared with the TF configuration studied in this work. The optimized TF aircraft has lighter fuel weight and gross weight compared to the optimized SBW aircraft, which is due to the fact that the TF aircraft has a lighter operational empty weight,

---

\* Presented as Paper 2023-2204 at the AIAA SciTech 2023 Forum, National Harbor, MD & Online, 23-27 January, 2023.

\* PhD student, Institute of Aircraft Design and Lightweight Structures; currently Postdoctoral Researcher at Visionary Aircraft Concepts, Bauhaus Aviation Research Institute, Willy-Messerschmitt-Straße 1, 82024 Taufkirchen, Germany; Yiyuan.Ma@bauhaus-luftfahrt.net

† Postdoctoral researcher, Institute of Aircraft Design and Lightweight Structures; currently assistant professor at the University of Wolverhampton, Department of Engineering, Telford, UK

‡ Professor, Computational Engineering and Design Group.

including lighter fuselage structural weight, landing gear weight, etc., whereas the top-level aircraft requirements are the same for both aircraft, including range, payload, and cruise Mach.

### Nomenclature

$AR$	=	aspect ratio
$C_D$	=	drag coefficient
$C_L$	=	lift coefficient
DOFs	=	degrees of freedom
$G$	=	parameters for Chebyshev polynomials
$G_{st}$	=	strut airfoil's scaling factor
$k$	=	fraction
$L_\delta$	=	roll moment due to an aileron deflection, N.m
$M_a$	=	Mach number
$M_{ff}$	=	fuel weight fraction
MTOM	=	maximum takeoff mass, kg
$n$	=	load factor
OEM	=	operating empty mass, kg
$P$	=	wing planform vector
$Q$	=	transformed and reduced material coefficient of the composite material
$U$	=	nodal displacement matrix
$m$	=	mass, kg
$X$	=	design variables vector
$\alpha$	=	angle of attack, deg
$\alpha_i$	=	incidence angle state variable, deg
$\Gamma$	=	vortex rings strengths
$\eta_\alpha$	=	aileron effectiveness
$\eta_{st}$	=	normalized spanwise strut attachment position
$\Lambda$	=	sweep angle, deg
$\lambda$	=	taper ratio

$\varphi$  = coupled adjoint vector

*Subscripts*

*AIC* = aerodynamic influence coefficient

*des* = design

*f* = friction

*fuse* = fuselage

*i* = induce

*p* = pressure

*RHS* = right-hand side

*W* = wing

## I. Introduction

Major aircraft manufacturers, such as Boeing and Airbus, forecast that the revenue passenger kilometer (measures the number of kilometers traveled by paying passengers) will maintain annual growth of more than 4% in the next few decades [1,2]. As the air transportation sector contributes a lot of greenhouse gases and other pollutants, including sulfur dioxide, nitrogen oxides, and noise, a step-change is required for the aviation industry to meet the stringent sustainable aviation goals set forth by NASA and the European Commission [3]. Since induced drag can account for up to 40% of the total drag of a medium-range aircraft similar to the A320 [4], the Ultra-High Aspect Ratio Wing (UHARW) concept is one of the keys to improving aircraft aerodynamic efficiency [5]. While the increased aerodynamic performance reduces aircraft fuel consumption, the bending moments and shear forces in the UHARW structure increase significantly with the conventional cantilever wing configuration, resulting in increased wing structural weight and reduced overall benefits of the UHARW concept [6].

Numerous promising configurations and technologies facilitate the application of UHARW, such as Twin-Fuselage (TF) [7–9], Strut-Braced Wing (SBW) [10–12], folding wingtip [13], and load alleviation [14]. Besides, advanced fiber-reinforced composite materials can be employed for wing structures to reduce structural mass [15]. The utilization of struts in the SBW configuration has the potential to substantially reduce the maximum bending moment experienced by the wing structure, often leading to reductions of up to 50% [16]. This in turn has a significant impact on reducing the wing weight, thereby increasing the wingspan and reducing the wing thickness and sweep angle [17]. For this reason, the SBW

configuration has been the subject of many recent studies on UHARW. For example, NASA's Subsonic Ultra-Green Aircraft Research (SUGAR) project performed comprehensive research on the medium-range SBW aircraft configuration [18]. Virginia Polytechnic and State University conducted the conceptual study and Multidisciplinary Design Optimization (MDO) for a long-range SBW aircraft [19]. Secco and Martins [20] employed a high-fidelity aerodynamic optimization method to minimize the drag of a transonic SBW aircraft. The outcome of this optimization was a notable 15% reduction in drag for the optimized configuration. The TF configuration facilitates UHARW design by utilizing off-centerline located fuselages. In addition, the TF transport aircraft makes better use of fuselage volume than the single wide-body configuration, allowing for significant reductions in fuselage structural mass [7]. The TF configuration has been realized and flight-tested on different types of aircraft, such as the general aircraft HY4 [21], a TF UAV [22,23], and Stratolaunch carrier aircraft [24]. A TF aircraft preliminary case study with similar parameter values to the reference conventional aircraft was presented by Chiesa et al. [8]. Vedernikov et al. [9] studied the TF aircraft employing a case study design based on the prototype of the A320 and described the drawbacks of the conventional single-fuselage configuration. Moreover, there are a few studies on the aerodynamic optimization [20,25,26] and MDO [27–30] of the TF and SBW configurations. However, these methods are too complex and time-consuming for the conceptual design phase, or too simplistic and only suitable for the initial sizing stage. In a previous study by the authors, TF and SBW configurations for different missions were studied through a comparative study at the conceptual design level by employing conceptual design tools and semi-empirical methods [5]. Considering the lack of real aircraft data for reference and verification, it is difficult to accurately investigate the characteristics of these unconventional configurations at the conceptual design stage. Therefore, this paper extends the comparative study to the preliminary design level, but includes higher-fidelity aerostructural optimization in order to provide a more comprehensive understanding of these unconventional configurations and to provide a reliable reference for the aircraft design community.

The gradient-based optimization approach is more effective than the heuristic optimization approach in most aerostructural optimization problems with a large number of design variables [31]. Besides, the coupled adjoint derivative analysis method can effectively compute the derivative of the coupled aerostructural optimization problems by solving the linearized governing equations [32]. Gray and Martins [33] employed the adjoint derivative analysis method for a highly flexible wing aerostructural optimization. Martins et al [34] performed high-fidelity aerostructural optimization for the wing of a

large transport aircraft by utilizing the adjoint method.

UHARW is more flexible than conventional wings and will exhibit larger deformation. This is especially true when they are made of composite materials, which, depending on their fiber orientation, may experience higher strains compared to traditional metallic materials [35]. Therefore, due to the high flexibility, UHARW has geometrically nonlinear behaviors that cannot be accurately analyzed with a linear structural model. If a linear model is used, this can lead to inaccurate wing structural sizing due to inaccurate linear stress calculation and inaccurate wing deflection, which will further affect the aerodynamic load distribution analysis [33].

Natural Laminar Flow (NLF), which maintains the wing planform and airfoil shape with a favorable pressure distribution, is one of the most promising methods for reducing aircraft drag [36]. Through a comparison of turbulence and NLF aircraft for mid-range transport missions, Xu and Kroo [37] investigated the advantages of NLF design. However, there are still significant challenges to the successful application of the NLF technique. Numerous wind tunnel and flight tests have shown that to achieve NLF design, the flight Mach number, wing sweep angle, and Reynolds number need to be constrained [38]. Regarding an acceptable compromise of wave and viscous drags and the accurate prediction of the laminar-turbulence transition, aerodynamic shape optimization and aerostructural optimization of swept NLF wings in the transonic region remain hard [39].

In this paper, a coupled adjoint aerostructural optimization tool FEMWET [40], consisting of a geometrically nonlinear structural model and a Quasi-three-Dimensional (Q3D) NLF aerodynamic solver, is used for the wing aerostructural optimization of the TF and SBW aircraft configurations. Two medium-range mission aircraft, one TF and one SBW, are designed as baseline reference configurations. An aeroelastic and an aerostructural optimization are carried out for these two aircraft with the objective function of minimizing fuel weight, respectively.

The rest of the paper is organized as follows: the methodology of the coupled adjoint aerostructural optimization and the verification are presented in Sec. II. Sec III shows the baseline configurations of the TF and SBW aircraft configurations. The aerostructural optimization for the two aircraft is performed and the results are discussed in Sec. IV. Finally, Sec. V provides a comprehensive conclusion.

## **II. Methodology for Coupled Adjoint Aerostructural Optimization**

The geometrically nonlinear coupled adjoint aerostructural optimization tool FEMWET, developed by the authors in Refs. [40,41], is used to perform aerostructural optimization for the MR-TF and MR-SBW

aircraft in this work. FEMWET includes a finite beam element structural solver and a Q3D aerodynamic solver. The coupled system is solved by using the Newton method. In this paper, FEMWET is modified and extended for the aerostructural optimization of TF and SBW aircraft configurations.

#### **A. Geometrically Nonlinear Structural Solver**

The structural analysis model is based on composite thin-walled beams with assumptions specific to UHARW, which was published by the authors in Refs. [40,42]. The adopted assumptions include:

- a) The UHARW is assuming free warping. The resultant moment (bimoment) due to the twist is negligible meaning that the rate of the twist angle along the beam axis is constant
- b) In-plane warping is not taken into account, which means the cross-section might not deform in its plane. Due to the existence of stiffening components like ribs and stringers, the cross-sectional deformation of aircraft wings remains minimal.
- c) As long as the twist angles are minor for the aerodynamic performance of the wing, small to moderate twist angles are taken into account in the calculation of the structural response for a wing. But using the approach, the finite element code can be extended to account for arbitrary large twist angles.
- d) The in-plane deformation is taken into account and the transverse shear deformation is added. Transverse shear strains in highly flexible composite UHARW are anticipated to no longer be negligible as in many conventional thin-walled composite beam models.
- e) It is assumed that the flexural displacements are tiny yet finite. Von-Karman-type strains are taken into consideration because nonlinear factors in transverse shear strains are disregarded. This presumption forms the basis of the formulation for the study of aircraft wing bending loads.

The wing cross-sections are represented by the wing box, solved by the finite element equations taking into account the large displacement analysis of composite thin-walled beams and the above-mentioned assumptions.

A brief introduction of the methodology is provided here, and the full formulation is derived and presented in Ref. [42]. The validation examples in Ref. [42] show that the proposed geometrically nonlinear model can predict small and large displacements of a thin-walled composite beam with acceptable accuracy.

## B. Aerodynamic Analysis Considering Natural-Laminar-Flow

FEMWET utilizes a Q3D aerodynamic solver [43], composed of a Vortex Lattice Method (VLM) code and the Two-Dimensional (2D), compressible airfoil analysis tool MSES [44], for wing aerodynamic analysis. The wing lift coefficient, spanwise lift distribution, and induced drag are calculated using the VLM code. The Prandtl-Glauert compressibility correction is used to correct the VLM calculation for the compressibility effect at a high Mach number.

To improve the aerodynamic analysis fidelity, the wing is divided into several sections for 2D aerodynamic analysis using MSES. The lift coefficient computed using the VLM code is interpolated to obtain the lift coefficient at each section along the wing span. Velocity, lift coefficient, and Mach number perpendicular to the wing sweep line are calculated using sweep theory. An incidence angle state variable ( $\alpha_i$ ) is used in 2D aerodynamic analysis to match the lift coefficient obtained by using MSES against that computed by using the VLM. The wing viscous, pressure, and wave drag are obtained by integrating the ones calculated by 2D aerodynamic analysis along the wingspan. In addition, the sensitivity of the wing lift and drag with respect to the wing geometry and angle of attack are computed by using MSES.

The inviscid flow results are coupled with compressible, integral boundary layer formulations featuring envelop  $e^N$  boundary layer transition prediction criterion in MSES through the displacement thickness and edge velocity. Newton method is used to solve the system of equations. Therefore, MSES can project the airfoil's laminar-to-turbulent transition points and compute the airfoil lift and drag coefficients in the free-transition mode. The accuracy of MSES in predicting laminar-turbulent transition has been validated through both numerical and experimental methods. In flight tests conducted by Youngren [45], the flight-test transition positions from the hot-film sensor closely match the MSES computation results, showing laminar flow up to at least 58% chord length. Lasauskas [46] compared the MSES-calculated results with measured data and demonstrated that the envelope of computed individual frequencies closely aligns with the measured data in the transitional region, encompassing both the attached boundary layer and the separated laminar shear layer. Wu et al. [47] conducted a comparison of transition positions and lift/drag coefficients obtained from different solvers. The results indicated that MSES predicts flow transition positions with a deviation of less than 4% compared to the predictions of other solvers. In this work, the free-transition mode of MSES is used for the aerostructural optimization of NLF wings.

### C. Aerostructural Coupling

The presented Q3D, NLF aerodynamic solver and the geometrically nonlinear structural solver are integrated to solve the coupled problem of flexible UHARW by using the Newton method. The coupled aerostructural system is characterized by the system of governing equations:

$$\begin{bmatrix} A(X, \Gamma, U, \alpha) \\ S(X, \Gamma, U) \\ W(X, \Gamma) \\ C(X, \Gamma, U, \alpha, \alpha_i) \end{bmatrix} = 0 \quad (1)$$

The first two equations represent the governing equations of the VLM and FEM, respectively. The third equation states that the lift should be equal to the design load factor times the aircraft design weight, which determines the wing's angle of attack. The fourth equation represents that the 2D sectional lift calculated by MSES should equal the lift computed by VLM. The Newton method is utilized to solve Eq. (1). The state variables  $[\Gamma, U, \alpha, \alpha_i]$  are updated iteratively by solving the following equation until Eq. (1) is fulfilled with a defined tolerance.

$$\begin{bmatrix} \frac{\partial A}{\partial \Gamma} & \frac{\partial A}{\partial U} & \frac{\partial A}{\partial \alpha} & \frac{\partial A}{\partial \alpha_i} \\ \frac{\partial S}{\partial \Gamma} & \frac{\partial S}{\partial U} & \frac{\partial S}{\partial \alpha} & \frac{\partial S}{\partial \alpha_i} \\ \frac{\partial W}{\partial \Gamma} & \frac{\partial W}{\partial U} & \frac{\partial W}{\partial \alpha} & \frac{\partial W}{\partial \alpha_i} \\ \frac{\partial C}{\partial \Gamma} & \frac{\partial C}{\partial U} & \frac{\partial C}{\partial \alpha} & \frac{\partial C}{\partial \alpha_i} \end{bmatrix} \begin{bmatrix} \Delta \Gamma \\ \Delta U \\ \Delta \alpha \\ \Delta \alpha_i \end{bmatrix} = - \begin{bmatrix} A(X, \Gamma, U, \alpha) \\ S(X, \Gamma, U) \\ W(X, \Gamma) \\ C(X, \Gamma, U, \alpha, \alpha_i) \end{bmatrix} \quad (2)$$

It should be emphasized that at each Newton iteration, the loads are calculated and transformed on the deformed geometry of the wing.

Aileron effectiveness is an important constraint in wing aeroelastic and aerostructural analysis, which is usually an active constraint [48], especially for the UHARW configuration. In this work, the aileron deflection is simulated in the VLM code and the aileron effectiveness is defined as:

$$\eta_\alpha = \frac{L_{\delta_{\text{elastic}}}}{L_{\delta_{\text{rigid}}}} \quad (3)$$

where  $L_{\delta_{\text{elastic}}}$  is the roll moment of the elastic wing due to an aileron deflection and  $L_{\delta_{\text{rigid}}}$  is the roll moment of the rigid wing due to an aileron deflection.

### D. Sensitivity Analysis

A gradient-based optimization algorithm is used for aerostructural optimization. For improving the optimization efficiency, the coupled adjoint derivative calculation method is used for the sensitivity

analysis. For the aerostructural problem defined in Eq. (3), the total derivative of a function  $I$  with respect to a design variable  $X$  is computed as

$$\frac{dI}{dX} = \frac{\partial I}{\partial X} - \varphi_1^T \left( \frac{\partial A}{\partial X} \right) - \varphi_2^T \left( \frac{\partial S}{\partial X} \right) - \varphi_3^T \left( \frac{\partial W}{\partial X} \right) - \varphi_4^T \left( \frac{\partial C}{\partial X} \right) \quad (4)$$

where  $\varphi = [\varphi_1 \ \varphi_2 \ \varphi_3 \ \varphi_4]^T$  is the adjoint vector, which is computed by:

$$\begin{bmatrix} \frac{\partial A}{\partial \Gamma} & \frac{\partial A}{\partial U} & \frac{\partial A}{\partial \alpha} & \frac{\partial A}{\partial \alpha_i} \\ \frac{\partial S}{\partial \Gamma} & \frac{\partial S}{\partial U} & \frac{\partial S}{\partial \alpha} & \frac{\partial S}{\partial \alpha_i} \\ \frac{\partial W}{\partial \Gamma} & \frac{\partial W}{\partial U} & \frac{\partial W}{\partial \alpha} & \frac{\partial W}{\partial \alpha_i} \\ \frac{\partial C}{\partial \Gamma} & \frac{\partial C}{\partial U} & \frac{\partial C}{\partial \alpha} & \frac{\partial C}{\partial \alpha_i} \end{bmatrix}^T \begin{bmatrix} \varphi_1 \\ \varphi_2 \\ \varphi_3 \\ \varphi_4 \end{bmatrix} = \begin{bmatrix} \frac{\partial I}{\partial \Gamma} \\ \frac{\partial I}{\partial U} \\ \frac{\partial I}{\partial \alpha} \\ \frac{\partial I}{\partial \alpha_i} \end{bmatrix} \quad (5)$$

All the partial derivatives in Eq. (5) are computed by a combination of analytical methods and automatic differentiation. The automatic differentiation is carried out by using the Matlab toolbox Intlab [49].

### E. Performance Analysis

The fuel mass minimization is used as the objective function in the aerostructural optimization, which is estimated by using the semi-empirical method presented in Ref. [50]. The Breguet range equation is employed to estimate the cruise-required fuel mass and statistical factors are utilized to calculate the other flight segments' fuel mass.

The aircraft lift-to-drag ratio is required to estimate the fuel mass. The total drag of the aircraft is assumed as the sum of the wing drag and the drag of the rest components of the aircraft. The wing drag is computed corresponding to the wing design variables, while the remaining drag (cruise angle of attack) is obtained from the conceptual design results and is kept constant during the optimization.

### F. Validation

In previous studies, FEMWET has been validated from different aspects. The accuracy of the Q3D aerodynamic solver was validated by utilizing a higher-fidelity CFD tool called MATRICS-V for drag prediction. The MATRICS-V has been validated using wind tunnel tests and flight test results. The Q3D solver and the MATRICS-V code computed the different drag components of the wing drag for the Fokker 100 in full turbulence under cruise conditions to validate the Q3D solver [41]. The computational results, as illustrated in Fig. 1, provide confirmation of the Q3D solver's high accuracy in drag prediction.

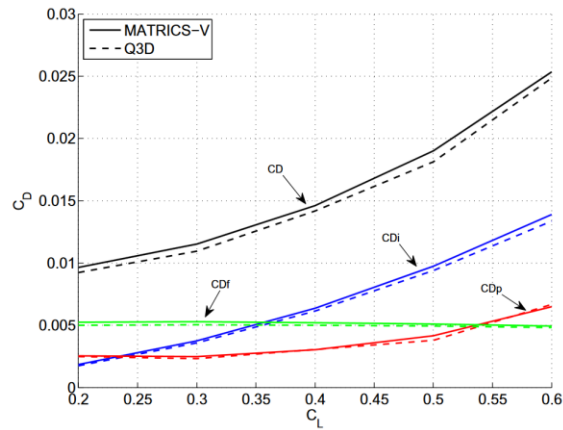


**Fig. 1 Comparison of calculated drag by the Q3D and MATRICS-V solvers for cruise condition (1 g load case and  $Ma=0.75$ ) [41].**

The A320-200 aircraft’s wing twist was utilized to validate the accuracy of the presented tool for computing the wing stiffness and deformation. An aeroelastic optimization was performed to determine the equivalent panel thickness and project the A320’s wing twist. Fig. 2 compares the A320 wing twist from FEMWET with the actual distribution, revealing an 8.5% maximum error at the wing tip [48].

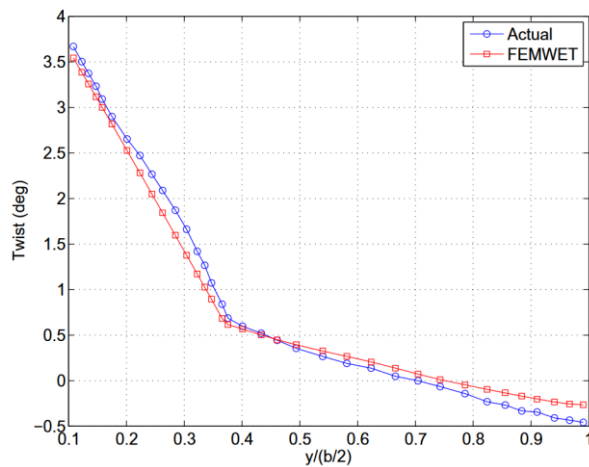


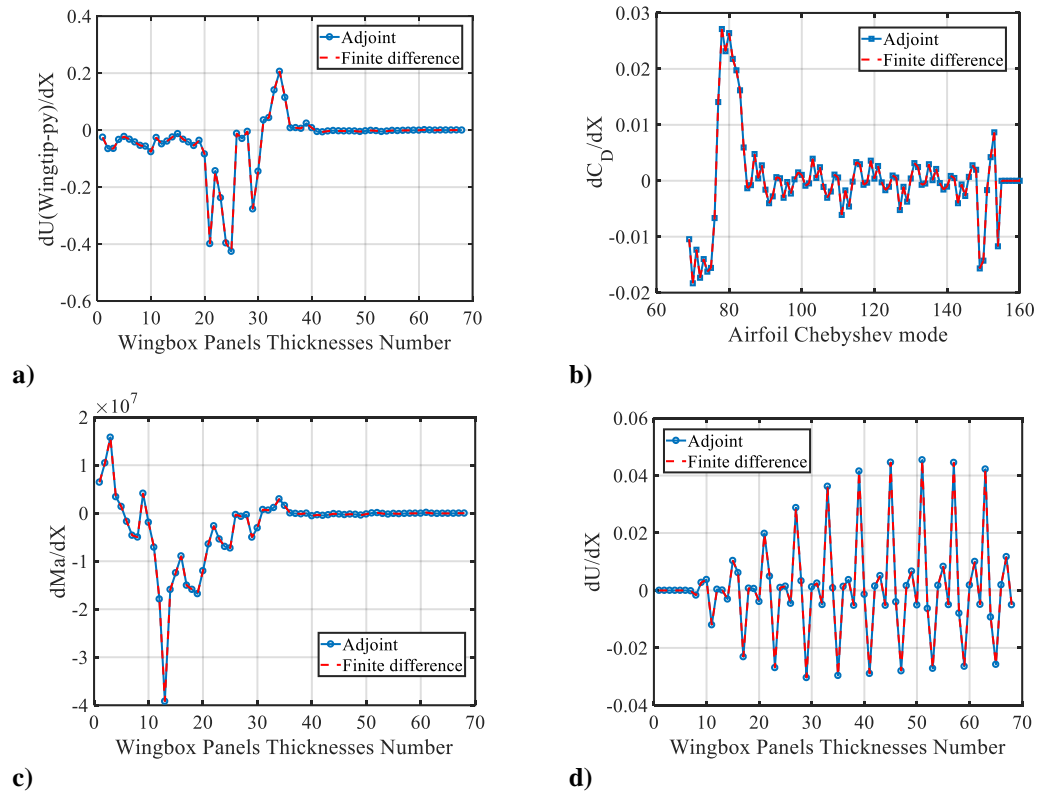
**Fig. 2 A320-200 wing twist under 1 g load [48].**

To validate FEMWET’s structural mass estimation accuracy, an aeroelastic optimization was conducted for the A320 aircraft wing and horizontal tail. Table 1 presents the comparison of their masses, revealing that the calculated values closely align with the A320-200’s reference values, showing less than a 1% error [31].

**Table 1 A320 mass validation**

Component	Reference	FEMWET	Error
Wing	8801 kg	8861 kg	0.68%
Horizontal tail	625 kg	619 kg	0.96%

The geometrically nonlinear structural analysis model has been validated in Ref. [40] by predicting large deflections of composite beams. Besides, the wing of the A320 aircraft was utilized to verify the correct implementation of the geometrically nonlinear composite version of FEMWET in Ref. [40]. A quasi-isotropic layup was employed for the wing box and the aeroelastic optimization showed reasonable results in comparison with references. The adjoint sensitivity analysis method employed in this study is validated by using the finite difference method for the structural model and the aerodynamic solver, respectively, as shown in Fig. 3.

**Fig. 3 Verification of the sensitivity analysis method.**

### III. Baseline Reference Aircraft

Medium-range TF and SBW aircraft configurations have been studied by the authors in the conceptual design phase in Ref. [5], both of which showed significant fuel efficiency improvements over the reference aircraft A320neo. Uncertainty analysis and constrained optimization were performed for these

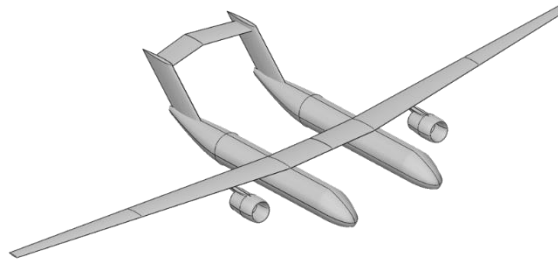
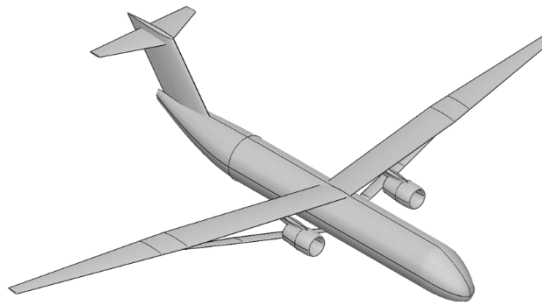
aircraft with an objective function of mission fuel mass [51]. The results of the uncertainty analysis indicate that the TF and SBW aircraft achieve the highest fuel efficiency when operating at a cruise Mach number of 0.735, within the uncertainty bounds ranging from Mach 0.71 to Mach 0.78. Additionally, this relatively low Mach number promotes the realization of NLF over the wing, resulting in further enhancements in the aircraft's fuel efficiency. Therefore, in this work, the TF and SBW aircraft were re-sized for the cruise Mach 0.735 as the baseline configuration for aerostructural optimization by using the conceptual design framework presented in Ref. [5].

Numerous studies on cutting-edge technologies are being done for the next-generation transport aircraft in the areas of aerodynamics, structures, control, materials, and so on [52]. These advanced technologies are expected to be applied to the next-generation transport aircraft to minimize emissions in the coming decades [53]. Since the TF and SBW aircraft investigated in this work are designed to enter service in 2040, the ultimate load factor requirement is anticipated to be reduced to  $+1.5\text{ g}/-0.5\text{ g}$  due to the application of advanced load alleviation techniques [5].

The top-level aircraft requirements are listed in Table 2. The aircraft conceptual design and analysis framework presented in Ref. [5] was used for the initial sizing and performance analysis of the MR-TF and MR-SBW aircraft. The designed aircraft was visualized using OpenVSP, as shown in Fig. 4 and Fig. 5. The wing geometry parameters and weight data of the MR-TF and MR-SBW aircraft are given in Table 3 and Table 4. It is noteworthy that the wingspan of both aircraft under investigation should not exceed 36 meters according to the International Civil Aviation Organization (ICAO) Class C restriction. The mass penalty associated with the wing folding mechanism is assessed employing the approach presented in Ref. [19]. This mass penalty remains constant and is independent of the bending moment at the wing section throughout the aerostructural optimization process.

**Table 2 Top-level aircraft requirements**

Parameter	Unit	Value
Cruise Mach	--	0.735
Max. Mach	--	0.78
Passengers (2 classes)	--	150
Range	nm	3400
Contingency fuel	--	3%
Reserves		
Divert segment	nm	200
Hold (at 1500 ft)	min	10
Cruise altitude	ft	33000
Service ceiling	ft	38500
Takeoff field length	ft	<6400
Landing distance	ft	<4500
Wingspan	ft	<118

**Fig. 4 MR-TF aircraft configuration.****Fig. 5 MR-SBW aircraft configuration.****Table 3 Wing geometry parameters**

Parameter	MR-SBW	MR-TF
Aspect ratio	25.81	24.33
Quarter-chord sweep, deg	10.54	9.70
Span, m	62.0430	56.2736
Taper ratio	0.43	0.44
Folding position ( $b/2$ ), m	18	18
Dihedral, deg	-1.5	-1.5
Strut attachment position	0.4865	--

**Table 4 Weight data of the MR-SBW and MR-TF aircraft**

Parameter	MR-SBW	MR-TF	A320neo
MTOM, kg	67262	56155	79000
Fuel weight, kg	16117	12638	20980
OEM, kg	36925	29297	44300
Wing, kg	11180.0 (include strut)	8101.8	

**Table 5 Load cases of the MR-SBW and MR-TF aircraft**

Load case	Type	Weight	H, m	Ma	n, g
1	Pull-up	MTOM	7500	0.78	1.5
2	Pull-up	MTOM	0	0.58	1.5
3	Push-down	MTOM	7500	0.78	-0.5
4	Roll	$M_{des}$	4000	0.75	1
5	Cruise	$M_{des}$	10058	0.735	1

#### IV. Aerostructural Optimization Studies

In this section, FEMWET is modified for TF and SBW aircraft configurations and is used to perform aerostructural optimization for the MR-TF and MR-SBW aircraft presented in Sec. III.

##### A. Optimization Problem Definition

In order to achieve a better convergence in aerostructural optimization, an aeroelastic optimization was first performed to obtain the thickness of the wing box equivalent panels for the initial wing geometry, which was used as initial values for the subsequent full aerostructural optimization.

In aeroelastic and aerostructural optimization, constraints were applied for the equivalent panels of the wing (and strut, for SBW configuration) to ensure that the structure does not fail under tension, compression, and buckling loads of all the considered load conditions. Besides, there was one more constraint on the aileron effectiveness of the wing. Wing structural weight (and strut weight, for SBW configuration), including wing box weight and secondary wing structures weight, was calculated according to the obtained equivalent panels' thicknesses. A safety factor of 1.5 was implemented for all structural failures. In composite structures, strength varies due to material, environment, and damage sensitivity. In preliminary design, we size structures employing the cut-off strain for tensile, compressive, and shear modes of failure, determined by the worst-case scenario. Composite material allowables are computed utilizing these cut-off strains along with the 10% rule [54], which estimates mechanical properties from ply properties and direction percentages. A detailed explanation can be found in Ref. [55]. However, for the buckling mode, the equivalent buckling load for shear buckling of composite skin panels was used, i.e., the Engesser's formula [56]. The material properties utilized for the composite

layers are listed in Table 6, with reference to Ref. [57].

**Table 6 Material properties for the composite layers**

Parameter	Value
$E_1$ , GPa	146.78
$E_2=E_3$ , GPa	10.3
$G_{12}=G_{13}$ , GPa	6.2
$G_{23}$ , GPa	4.8
$\nu_{12}=\nu_{13}$	0.28

### 1. Aeroelastic Optimization Problem

The aeroelastic optimization's objective is to minimize the wing structural mass (and strut mass of SBW configuration) while ensuring that the structure satisfies the failure constraints under the specified load cases. The aeroelastic optimization problem is defined as:

$$\begin{aligned}
 & \text{minimize} && W_w(X) \\
 & \text{w.r.t.} && X = [t_{u_i}, t_i, t_{fs_i}, t_{rs_i}] \\
 & \text{subject to} && \text{Failure}_k \leq 0 \\
 & && 1 - L_\delta / L_{\delta, \min} \leq 0 \\
 & && X_{\text{lower}} \leq X \leq X_{\text{upper}}
 \end{aligned} \tag{6}$$

The wing (and strut) is divided into multiple trunks along the wingspan with four panels, including upper panels, lower panels, front spars, and rear spars. Each panel is divided into four elements for the stress and failure criteria computation, and each spar is divided into two elements for the same reason. The failure criteria are composed of failure under tension, compression, and Euler and shear buckling.  $L_\delta$  is the derivative of the roll moment due to the aileron deflection of the wing.  $L_{\delta, \min}$  is the minimum required roll moment due to aileron deflection to satisfy the roll requirements according to the regulations [58]. In this study, the aircraft's moment of inertia was calculated using Roskam's semi-empirical method [59], and the  $L_{\delta, \min}$  is calculated using Sadraey's method [58].

### 2. Aerostructural Optimization Problem

The objective of aerostructural optimization is to minimize the fuel weight according to Roskam's semi-empirical fuel weight estimation method [50], which is

$$W_F = k_R (1 - M_{ff}) MTOW \tag{7}$$

where  $k_R$  denotes the consideration of reserve fuel, which in this study is set to 1.03 according to the top-level aircraft requirements given in Table 2.

The aerostructural optimization problem is defined as:

$$\begin{aligned}
& \text{minimize} && W_F(X) \\
& \text{w.r.t.} && X = [t_{u_i}, t_{l_i}, t_{f_{s_i}}, t_{r_{s_i}}, G, P, W_{FS}, MTOW_S] \\
& \text{subject to} && \text{Failure}_k \leq 0 \\
& && 1 - L_\delta / L_{\delta, \min} \leq 0 \\
& && \frac{MTOW / S_w}{MTOW_0 / S_{w0}} - 1 \leq 0 \\
& && \frac{W_F}{W_{FA}} - 1 \leq 0 \\
& && \frac{W_F}{W_{FS}} - 1 = 0 \\
& && \frac{MTOW}{MOTW_S} - 1 = 0 \\
& && X_{lower} \leq X \leq X_{upper}
\end{aligned} \tag{8}$$

The design variables include the thickness of wing and strut (for SBW configuration) structural panels and spars, wing and strut (for SBW configuration) airfoil shapes, wing planform geometry, and two surrogate variables. The airfoil shape at the specific spanwise position is parameterized using Chebyshev polynomials. 20 modes are used for each airfoil, i.e., 10 modes for each airfoil surface. The wing planform geometry vector  $P$  includes wingspan, taper ratio, root chord, leading-edge sweep angle, and two twist angles at the kink and tip, respectively. Two surrogate variables, fuel weight and MTOM, are defined to avoid additional iterations between performance calculation and aerostructural analysis.

## B. Twin-Fuselage Aircraft

### 1. Aerostructural Optimization Study

The wing geometry of the TF aircraft is shown in Fig. 6. Due to the size constraints of airport infrastructure, the wing of the UHARW aircraft has been designed to fold up at the airport. The wing structural mass penalty due to the wing folding mechanism was estimated employing the semi-empirical method presented in Ref. [19], which was assumed to be constant in the optimization process. In order to mitigate the structural weight penalty, the fuel tank length ends at the wing folding position, and the available fuel volume is added as a constraint in the aerostructural optimization. The spacing between the two fuselages of the TF aircraft is limited to 9 meters for the medium-range mission due to the airport (ICAO Class C airports) facilities constraints [18], and the wing kink is in the same position.

The wing is modeled using finite beam elements in FEMWET. The wing box is replaced by a beam placed at the wing box's elastic axis. The equivalent beam is connected to the fuselage and has fixed DOFs at the connection, as illustrated in Fig. 7.

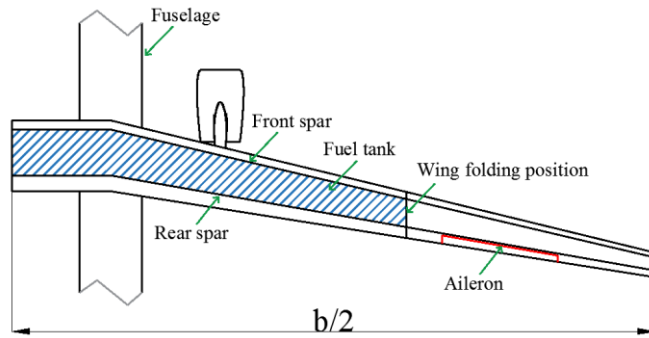


**Fig. 6 Schematic of the MR-TF aircraft wing**

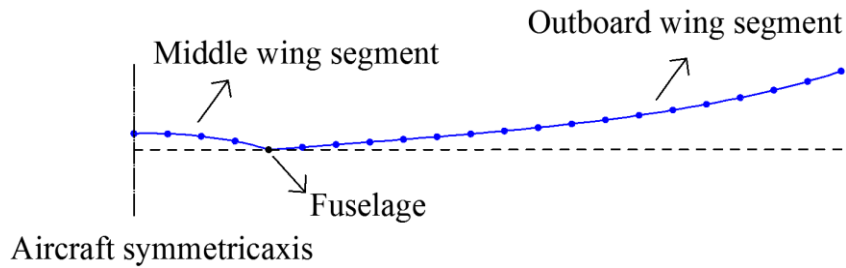


**Fig. 7 Wing beam models in FEMWET of TF aircraft under the positive load condition (dash line represents jig shape).**

In order to improve the computation efficiency, only the half wing of the TF aircraft is modeled in FEMWET. Since the symmetry plane of the wing is in the middle of the inboard wing segment, its boundary conditions need special attention. As listed in Table 5, the load cases (i.e., flight conditions) including both symmetrical maneuvering flight and anti-symmetrical maneuvering flight (i.e., rolling motion), symmetry and anti-symmetry boundary conditions need to be applied to the symmetry plane of the TF aircraft's wing in terms of different flight conditions. The boundary conditions used for the TF aircraft's wing are illustrated in Fig. 8. The deformation of the initial wing of the TF aircraft under different load cases is shown in Fig. 9.

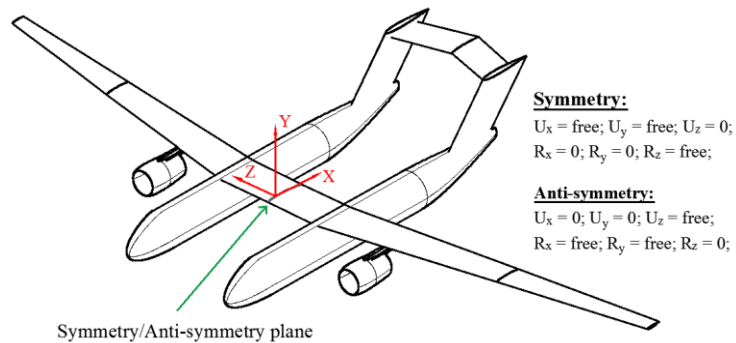


**Fig. 8 Illustration of the TF aircraft wing's boundary conditions.**



aircraft, as listed in Table 5. Besides, four additional constraints were included in the aerostructural optimization problem, i.e., wing loading, available fuel volume, and two equality constraints applied for the two surrogate variables. In summary, a total of 2213 constraints were used in the aerostructural optimization, as tabulated in Table 8.

As listed in Table 7 and Table 8, for the aerostructural optimization problem studied in this research, the number of constraints is more than the number of design variables. In this case, the direct method is more efficient than the adjoint method. We initially created the code for this work using the adjoint method and the constraint aggregation methodology. However, after testing, we found that its extremely high computational efficiency, so in order to strengthen the optimization's robustness, we applied all of the constraints directly rather than aggregating them at the time when the adjoint method's cost was still manageable (the CPU time for solving the 2213 adjoint equations was under 3 seconds).

**Table 7 Number of design variables of the TF aircraft aerostructural optimization**

Design variable	Number
Thicknesses of wing upper panel	10
Thicknesses of wing lower panel	10
Thicknesses of wing front spar	10
Thicknesses of wing rear spar	10
Wing airfoil Chebyshev polynomials	100
Wing planform geometry	6
Surrogate variable	2
<b>Total</b>	<b>148</b>

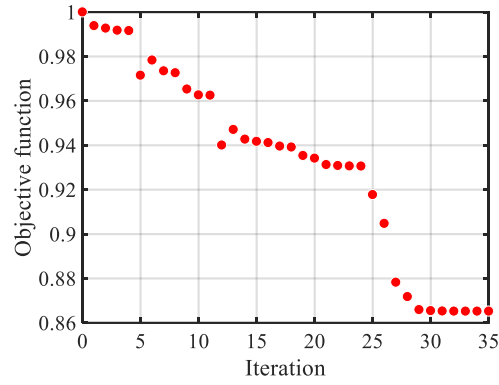
**Table 8 Number of constraints of the TF aircraft aerostructural optimization**

Constraint	Number
Tension	552
Compression	552
Buckling	1104
Aileron effectiveness	1
Wing loading	1
Fuel volume	1
Surrogate variable	2
<b>Total</b>	<b>2213</b>

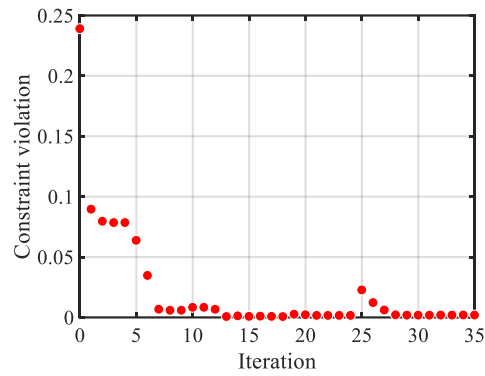
The load cases considered in the aeroelastic and aerostructural optimizations are listed in Table 5. An aeroelastic optimization was first performed to obtain a reasonable wing structure. Then, the aerostructural optimization was carried out. The optimization history is shown in Fig. 10. The aerostructural optimization was conducted in the free-transition mode to consider the flow transition of the wing starting with the transonic NLF airfoil presented in Ref. [60]. As given in Table 9, The optimized

wing of the TF aircraft resulted in more than a 13% reduction in fuel mass, more than 14% reduction in MTOM, and more than a 10% reduction in wing structural mass. As shown in Fig. 11, the optimizer reduced the wing aspect ratio during optimization to reduce the wing structural mass and the mass penalty due to the aileron effectiveness constraint. Besides, the optimizer also reduced the wing sweep angle by removing/weakening shock waves, as illustrated in Fig. 12. Furthermore, since the wing airfoil shapes were modified in the free transition mode optimization to widen the laminar flow range over the wing, the wing friction drag was reduced by more than 53%, as listed in Table 9. As shown in Fig. 13, the extent of the laminar boundary layer on both the upper and lower surfaces of the wing has been greatly improved during the optimization.

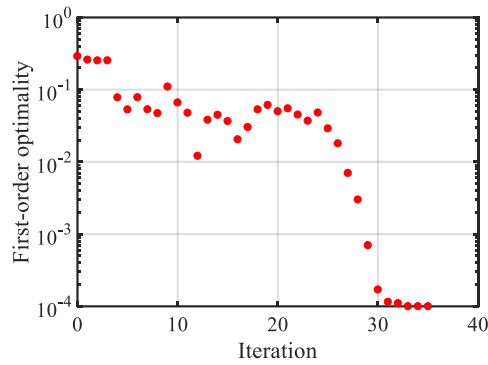
For comparison, an additional aerostructural optimization was performed, starting with the same airfoil but using a triggered transition mode, where the airflow transition is triggered at 2% of the chord from the wing leading edge to achieve a fully turbulent design. The two optimization results are compared in Table 9 and Table 10 and Fig. 11. The optimization in triggered transition mode resulted in a 7.87% and 9.68% reduction in the aircraft's fuel mass and MTOW, respectively. In the triggered transition mode, optimization led to a reduction in  $AR$  and an increase in the wing sweep angle, which stands in contrast to the outcomes observed in the free transition mode. This was done to minimize structural weight and total drag, with a particular focus on reducing wave drag. As a result, the aircraft's fuel weight is decreased.



a) Objective function



b) Constraint violation

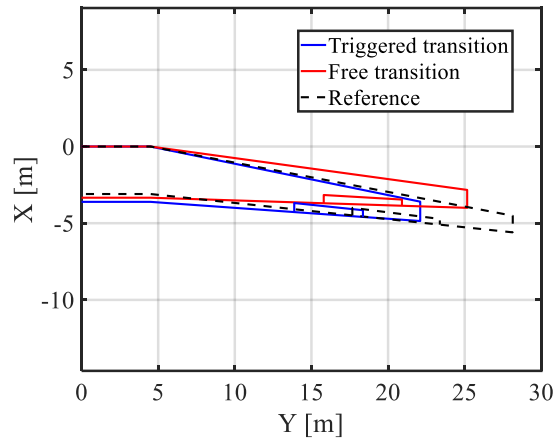


c) First-order optimality

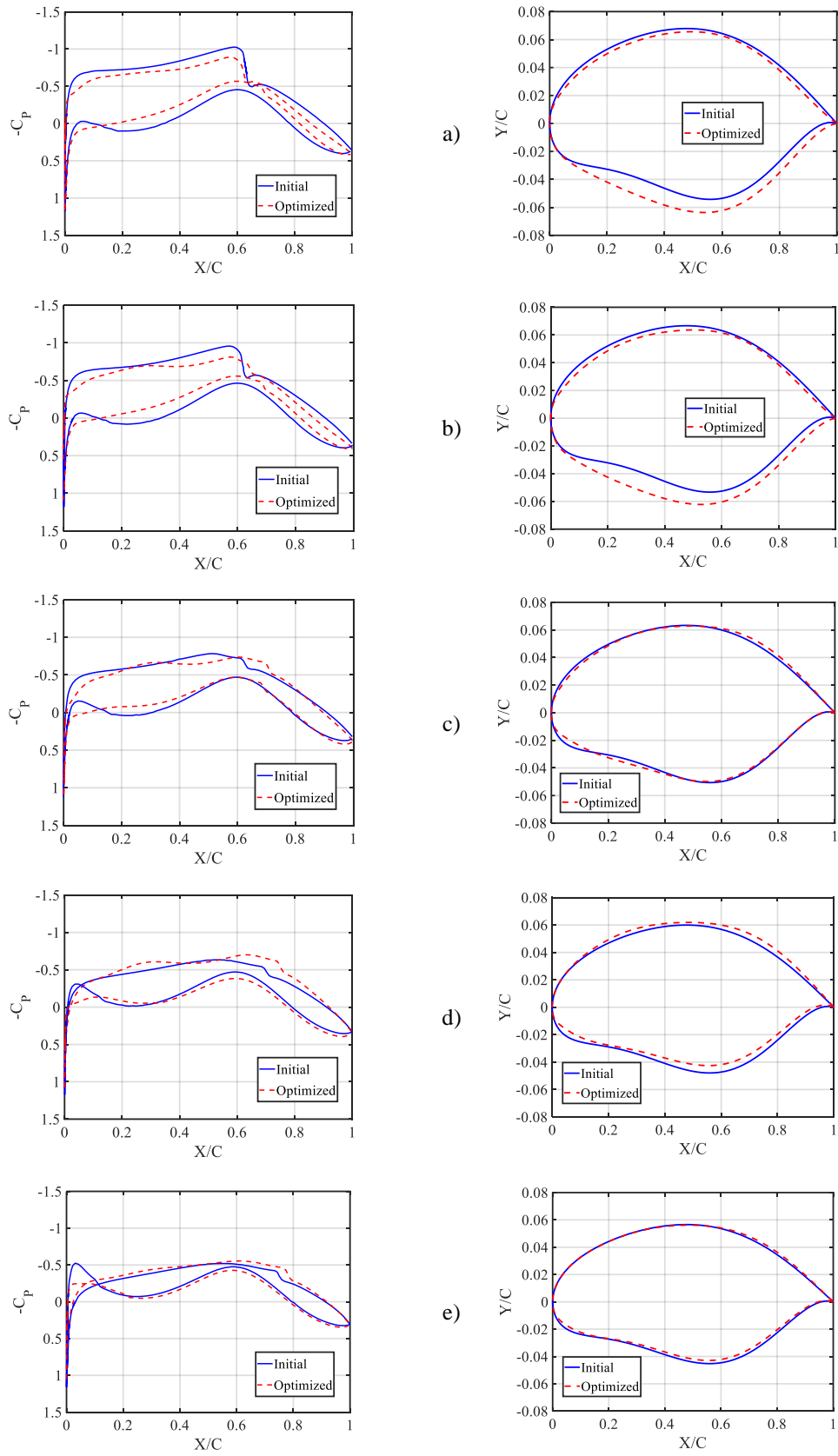
Fig. 10 History of the TF aircraft aerostructural optimization in free transition mode.

Table 9 Aerostructural optimization results of the TF aircraft

Configuration	$m_F$ , kg	MTOM, kg	$m_W$ , kg	$C_L$	$C_D$	$AR$	$\Lambda$ , deg
Baseline TF	12638	56155	8101.8	0.3863	0.0230	24.33	9.70
Free transition	10935	47758	7247.3	0.3400	0.0167	20.74	7.80
Triggered transition	11644	50721	5559.5	0.3802	0.0221	16.85	10.40



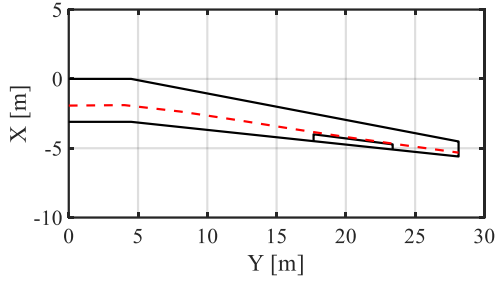
**Fig. 11 Wing planform comparison of the TF aircraft (fuselage is located at 4.5 meters of half wingspan).**



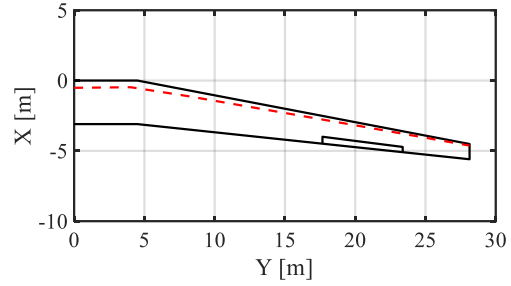
**Fig. 12 Pressure distribution and airfoil shape of the sections in different wing spanwise positions from root (a) to tip (e) of the TF aircraft (free transition mode).**

**Table 10 Wing drag breakdown of the TF aircraft**

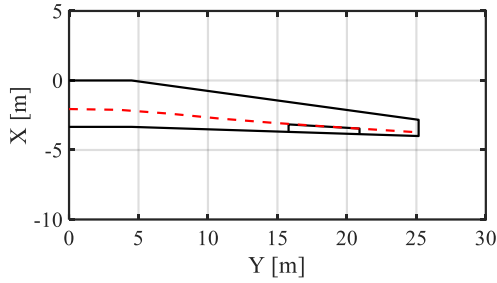
Configuration	$C_{D,w}$	$C_{Di,w}$	$C_{Df,w}$	$C_{Dp,w}$
Baseline TF	0.0110	0.0027	0.0052	0.0031
Free transition	0.0047	0.0017	0.0024	6.99e-4
Triggered transition	0.0101	0.0026	0.0052	0.0023



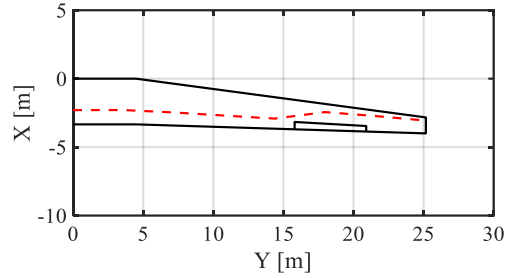
**a) Initial wing upper surface**



**b) Initial wing lower surface**



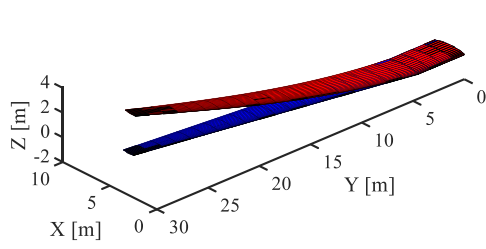
**c) Optimized wing upper surface**



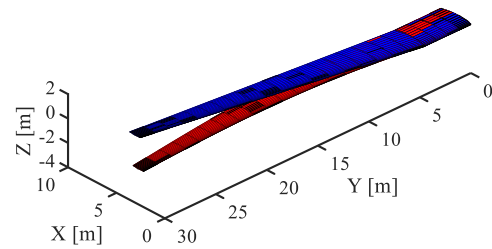
**d) Optimized wing lower surface**

**Fig. 13 Boundary layer transition profiles of the TF aircraft (fuselage is located at 4.5 meters of half wingspan; free transition mode).**

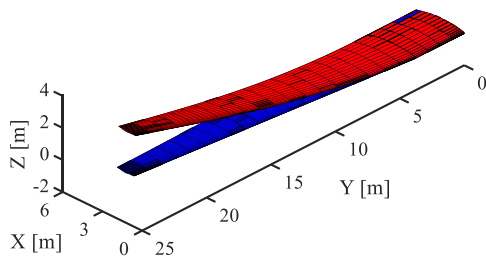
As listed in Table 10, the induced drag was reduced despite the decrease in the wing aspect ratio. This is due to the reduced cruise lift coefficient of the optimized aircraft and the fact that the optimizer tried to push the spanwise load distribution toward the elliptical lift distribution. The deformation of the initial wing and the optimized wing under two ultimate loads of pull-up and push-down are shown in Fig. 14. The optimizer reduced the thicknesses of the wing box panels and spars while reducing the wing aspect ratio so that the deformation of the optimized wing under the ultimate positive load case is similar to that of the initial wing, but the deformation under the ultimate negative load case is reduced.



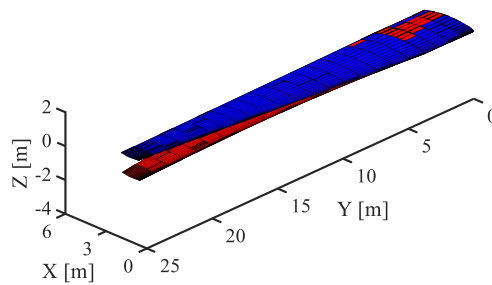
a) Initial wing under +1.5g



b) Initial wing under -0.5g



c) Optimized wing under +1.5g



d) Optimized wing under -0.5g

**Fig. 14** Wing deformed shape and jig shape of the TF aircraft under maximum pull-up and push-down loads (fuselage is located at 4.5 meters of half wingspan).

## 2. Influence of Wing Aspect Ratio on Wing Structural Weight

As the wing aspect ratio is one of the most important design parameters affecting the wing structural weight, this section investigates the influence of the wing aspect ratio on the wing structural weight of TF aircraft. By employing the aforementioned aeroelastic optimization method, five different aspect ratio wings of TF aircraft, ranging from  $AR$  10 to  $AR$  20, with the same wing reference area, were examined. Three of the investigated wings are shown in Fig. 15.

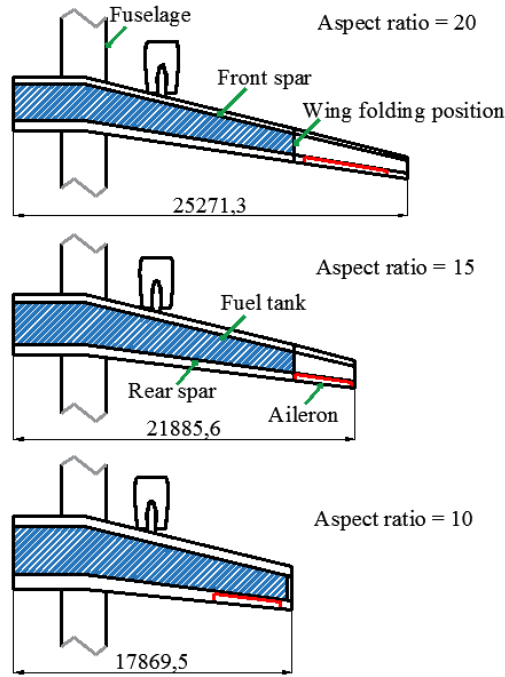


**Fig. 15 Schematic of different aspect ratio wings of the TF aircraft.**

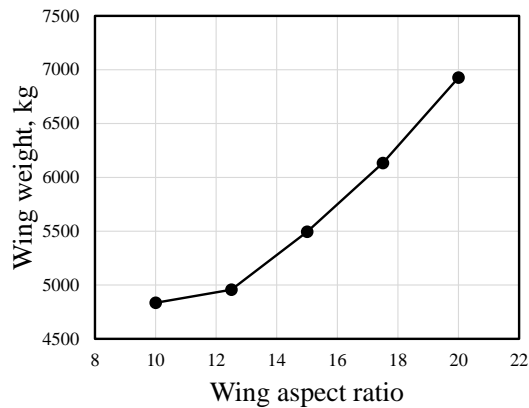


**Fig. 16 Change of TF aircraft wing structural weight with wing aspect ratio.**

As illustrated in Fig. 16, the TF aircraft wing structural weight increases exponentially with the wing aspect ratio. This implies that, in some cases, the wing structural weight penalty of a TF aircraft with the UHARW design may outweigh the aerodynamic gains, particularly when the snowball effect of the increased aircraft gross weight is taken into account. Therefore, a comprehensive evaluation of both the aerodynamic advantages and the wing structural weight penalty for the TF configuration with the UHARW design is required, i.e., the complete aerostructural optimization carried out in this paper.

The deflection and twist along the wing span of the optimized TF wings with different aspect ratios are shown in Fig. 17 and Fig. 18. The absolute values of both wing tip deformation and wing tip twist increase with the increase of wing aspect ratio. As illustrated in Fig. 18, The deformation and twist of

the middle segment of these wings with differing aspect ratio values are substantially smaller than that of the outboard wing segment because of the comparatively close distance between the two fuselages (all 9 meters according to the International Civil Aviation Organization airport infrastructure constraint [61]).

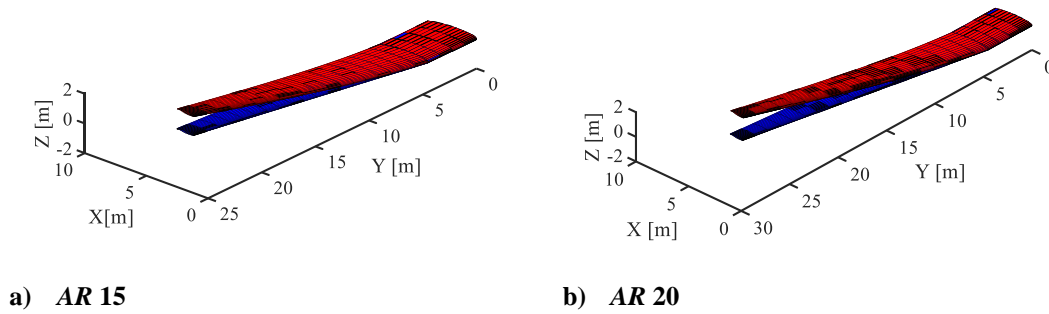
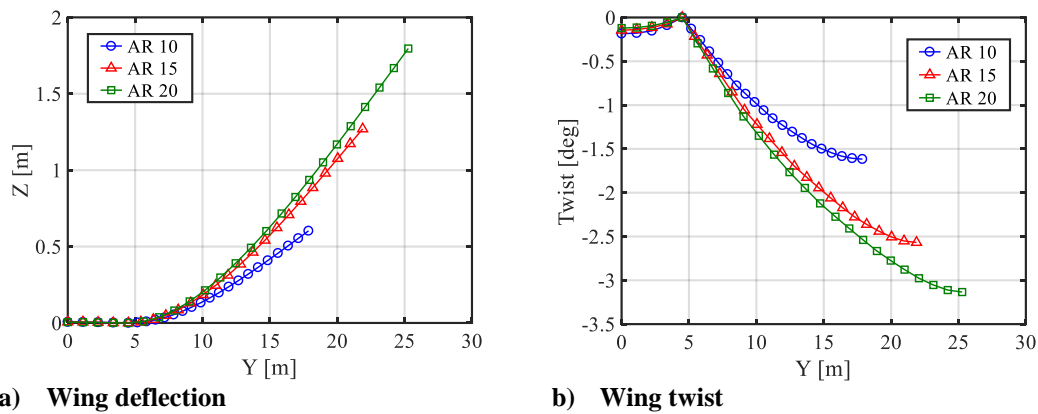


**Fig. 17 TF aircraft wing deflection with different wing aspect ratios under +1.5g load factor.**



**a) Wing deflection** **b) Wing twist**

**Fig. 18 TF aircraft wing deflection and twist with different wing aspect ratios under +1.5g load factor.**

### 3. Influence of Fuselage Spacing on Wing Structural Weight

Off-centreline-located fuselages are the main feature of the TF configuration. The fuselage spacing, i.e., the distance between the two fuselages, has a significant impact on the wing structural weight and the gross weight of TF aircraft. Therefore, the influence of the fuselage spacing on the wing structural weight of TF aircraft is investigated in this section. The wings of six TF aircraft with different fuselage spacing values (half span 4.5m to 9.5m) with the same wing reference area and aspect ratio (AR 20) were investigated by employing the aeroelastic optimization method presented in this paper. Two examples of the studied wings are illustrated in Fig. 19.

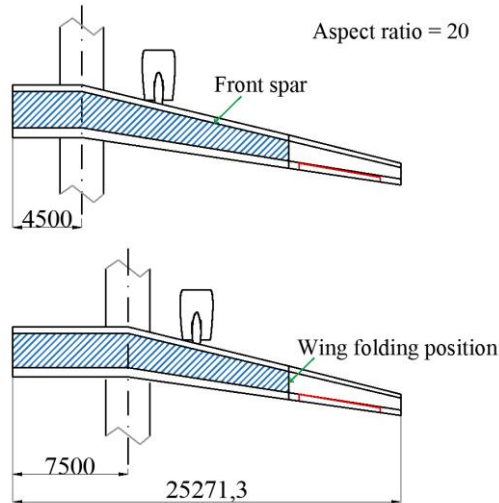


**Fig. 19 Schematic of different fuselage spacing of the TF aircraft.**

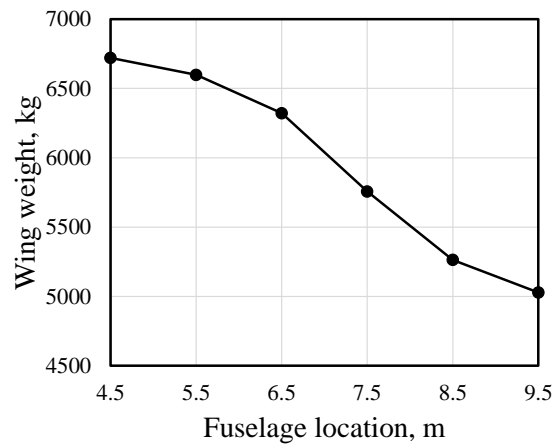
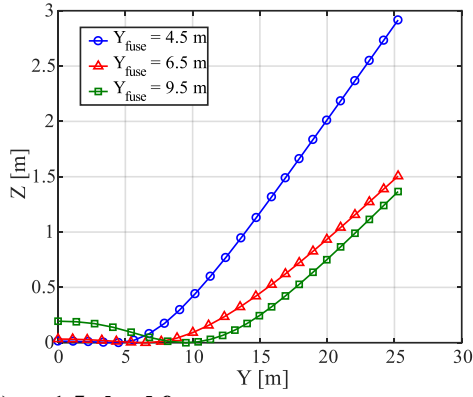


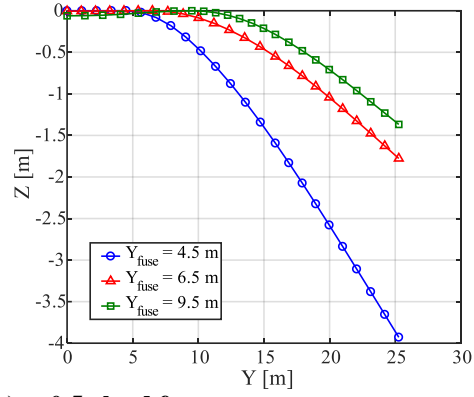
**Fig. 20 Change of TF aircraft wing structural weight with fuselage spacing.**

As shown in Fig. 20, the TF aircraft wing structural weight decreases with the increase of fuselage spacing. When the fuselage spacing increases from 4.5 m to 9.5 m of half-wing span, the wing structural weight decreases by 25.17%. It should be mentioned that when the fuselage spacing increases from 4.5m of half wing span, wing weight decreases rapidly at first, but when the fuselage spacing exceeds 8.5m of half wing span, the decrease of wing weight with respect to fuselage spacing gradually slows down. However, in reality, the fuselage spacing is subject to many constraints, including airport runway width, flight stability and maneuverability, etc.

The wing deflection of the optimized wings with different fuselage spacing values is shown in Fig. 21. With the increase of fuselage spacing, the vertical deformation of the outboard wing segment decreases significantly, while the vertical deformation of the middle wing segment (between the two fuselages) increases slightly.



a) +1.5g load factor



b) -0.5g load factor

**Fig. 21 Wing deflection of TF aircraft with different fuselage spacing.**

### C. Strut-Braced-Wing Aircraft

#### 1. Aerostructural Optimization Study

The wing geometry of the SBW aircraft is shown in Fig. 22. The same design as the TF aircraft, the SBW aircraft's wing is also designed to be foldable when operating at airports and the fuel tank length is limited by the wing folding position.

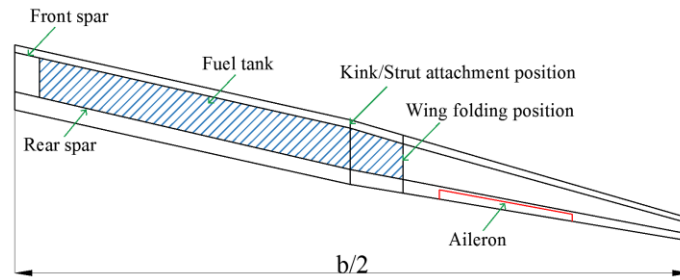


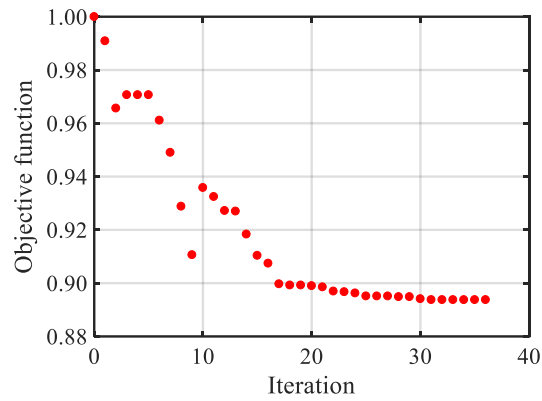
**Fig. 22 Schematic of the MR-SBW aircraft wing.**

NASA-funded research showed that for SBW aircraft with cruise Mach 0.80 or less, its struts are best designed as purely structural components with trimming to limit its drag contribution [62]. Therefore, in this work, the struts were designed as non-lifting surfaces with symmetric airfoils. Only the thickness-to-chord ratios of five strut cross-sections were selected as design variables.

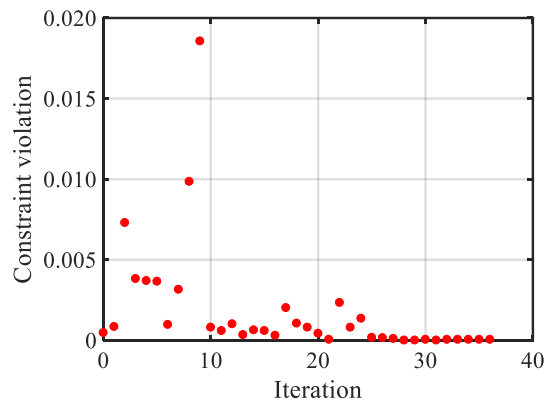
The wing and strut are modeled using finite beam elements, i.e., they are replaced by beams placed at the wing box's elastic axis position. The strut beam is connected to the corresponding wing beam node at the strut attachment position.

An aeroelastic optimization was first performed to obtain a reasonable wing structure. Then, the aerostructural optimization was conducted. In the SBW aerostructural optimization, a total of 201 design variables and 3077 constraints were utilized. The load conditions considered in the optimization are given

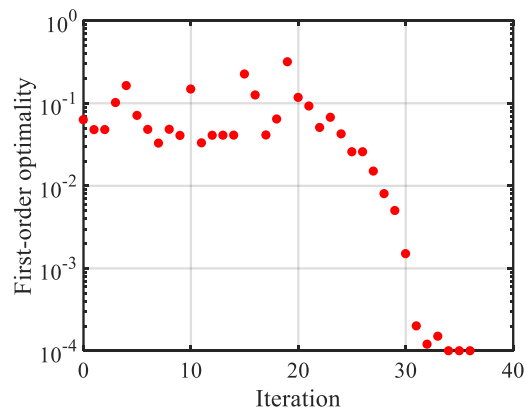
in Table 5. The same NLF airfoil was employed in the SBW optimization. The optimization history is shown in Fig. 23, and the optimization results are listed in Table 11. The aerostructural optimization in free transition mode resulted in a more than 10% reduction in fuel weight, more than 8% lower MTOM, and a more than 30% reduction in the wing and strut structural weight.



**a) Objective function**



**b) Constraint violation**



**c) First-order optimality**

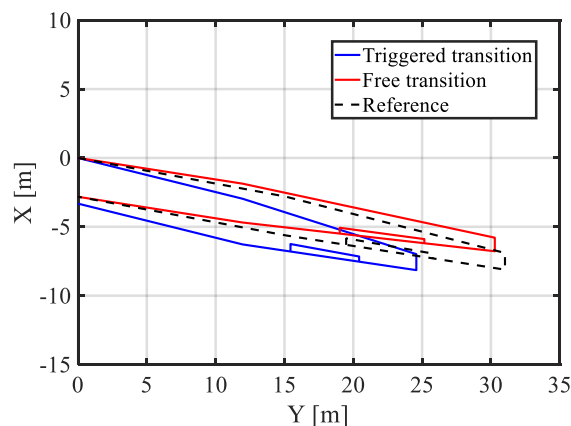
**Fig. 23 History of the SBW aircraft aerostructural optimization in free transition mode.**

**Table 11 Aerostructural optimization results of the SBW aircraft**

Configuration	$m_F$ , kg	MTOM, kg	$m_W$ , kg	$C_L$	$C_D$	$AR$	$\Lambda$ , deg
Baseline SBW	16117	67262	11180	0.3893	0.0229	25.81	10.54
Free transition	14406	61488	7735	0.3778	0.0175	26.01	8.88
Triggered transition	15302	62769	7500	0.3883	0.0221	17.37	13.92

As listed in Table 11, the optimizer slightly increased the wing aspect ratio in the free transition mode, which is keen to increase the wing structural mass. Therefore, the optimizer reduced the wing sweep angle (see Fig. 24) and made the optimized wing more flexible to mitigate the wing structural mass increment. As shown in Fig. 25, the wing airfoil shapes were adjusted to reduce the wave drag by removing/weakening shock waves, allowing the optimized wing to have a lower sweep angle. Moreover, since the wing airfoils were modified to widen the natural laminar flow range, the wing friction drag was lowered by more than 56%, as given in Table 12. As shown in Fig. 26, the optimized wing's laminar boundary layer range on the wing upper surface was improved by 10%, while a more significant improvement of the laminar flow range is found on the wing lower surface, which was increased by more than 200% inside the aileron and more than 100% outside the aileron along the wingspan.

An additional aerostructural optimization was performed in the triggered transition mode for the SBW for comparison purposes, starting with the same airfoil and triggering the airflow transition at 2% of the chord length. The two optimization results are compared in Table 11 and Table 12 and Fig. 24. The optimization in triggered transition mode reduced the fuel mass and aircraft MTOW by 5.06% and 6.68%, respectively. In line with the findings from the TF optimization, the optimization in triggered transition mode also involves a reduction in wing  $AR$  and an increase in the wing sweep angle to minimize structural weight and total drag.

**Fig. 24 Wing planform comparison of the SBW aircraft.**

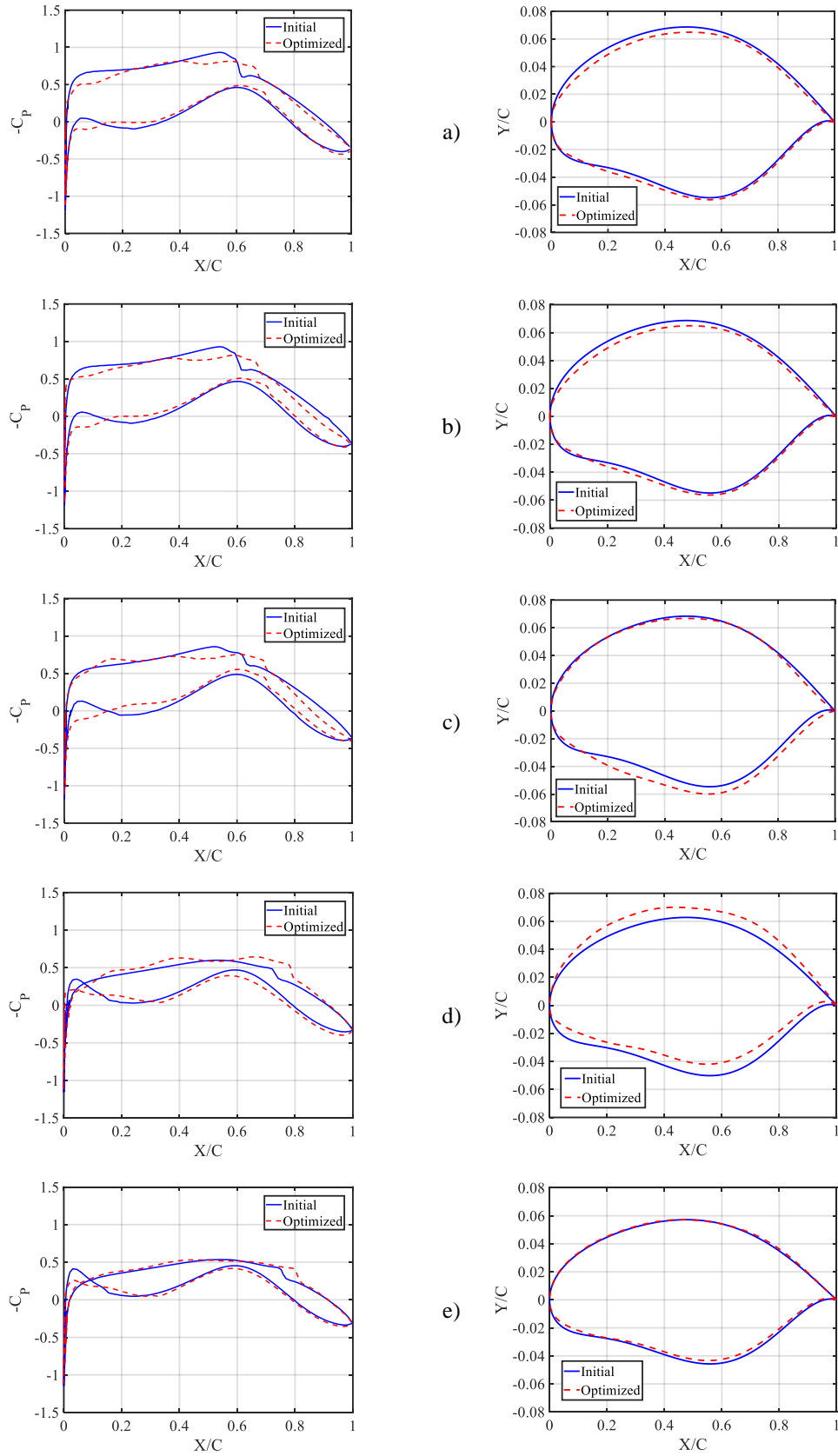


**Fig. 25 Pressure distribution and airfoil shape of the sections in different wing spanwise positions from root (a) to tip (e) of the SBW aircraft (free transition mode).**

**Table 12 Wing drag breakdown of the SBW aircraft**

Configuration	$C_{D,w}$	$C_{D_{i,w}}$	$C_{D_{f,w}}$	$C_{D_{p,w}}$
Baseline SBW	0.0101	0.0021	0.0052	0.0028
Free transition	0.0047	0.0017	0.0023	6.77e-4
Triggered transition	0.0093	0.0025	0.0050	0.0018

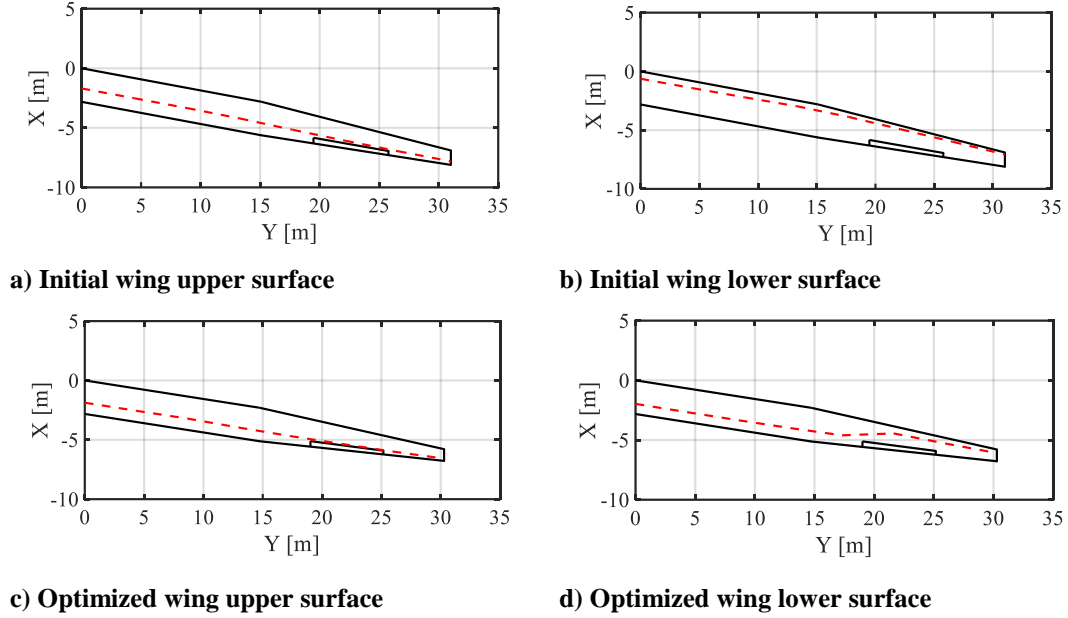


**Fig. 26 Boundary layer transition profiles of the SBW aircraft (free transition mode).**

## 2. Influence of Wing Aspect Ratio on Wing Structural Weight

The influence of wing aspect ratio on SBW structural weight has been studied by the authors in Ref. [42]. Similar to the TF study case, three SBWs with different aspect ratios and the same reference area were generated, as shown in Fig. 27. The wing structural weight, deflection, and twist are presented and described in Ref. [42]. The influence of the wing aspect ratio on SBW structural weight is shown in Fig. 28. It should be mentioned that as the wing aspect ratio increases, the aileron effectiveness constraint shows a more significant impact on the wing and strut structural weight. In addition, the rise in wing structural weight is greater than the increase in strut structural weight with an increase in wing aspect ratio.

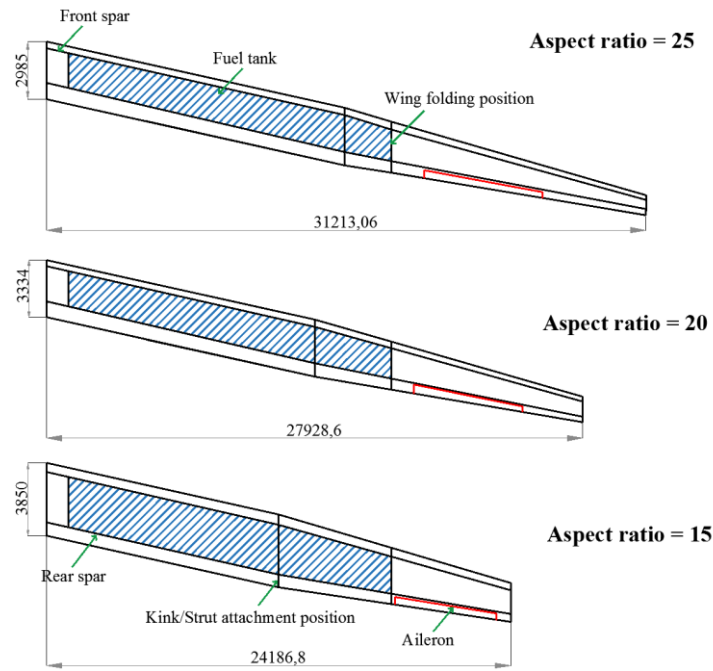


**Fig. 27 Schematic of the three different SBWs.**

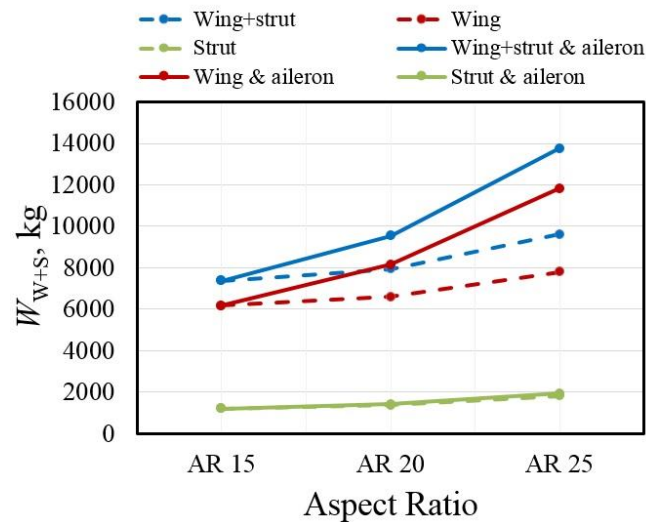


**Fig. 28 Change of SBW structural weight with wing aspect ratio.**

#### D. Comparison of Optimized Configurations

The TF and SBW configurations before and after aerostructural optimization are compared in Table 13. The aerostructural optimization proposed in this paper resulted in significant reductions in fuel mass and MTOM for both TF and SBW configurations. The optimized TF and SBW configurations exhibit remarkable reductions in fuel mass, with 48% and 31% lower values, respectively, in comparison to the A320neo, which serves as the original reference aircraft. Importantly, these substantial improvements can be ascribed not solely to aerostructural optimization but also to the integration of advanced technology assumptions made during the conceptual design phase. These include the adoption of NLF,

advanced composite materials, and load alleviation technologies, as described in Ref. [5]. The fuel mass and MTOM of the optimized TF aircraft are notably lighter than those of the SBW aircraft, mainly due to a better starting point (i.e., initial configuration) for the aerostructural optimization of the TF aircraft, as given in Table 4. This is because, in addition to the weight reduction of the wing structure, the fuselage weight of the TF configuration is also expected to be reduced, as given in Table 13. Since a pressure cabin's skin thickness is proportional to its volume, TF aircraft's two fuselage skins together will weigh the same as that of the conventional single-fuselage aircraft divided by  $\sqrt{2}$  if the TF aircraft's cabins are designed to have the same total floor area as conventional single-fuselage aircraft [27]. Furthermore, although an additional nose landing gear is needed, the TF configuration offers the optimal location for the main landing gear. The main landing gear's exterior fairings are not necessary for the TF configuration, and the main landing gear's strut length and mechanics can be shortened and made simpler, which helps reduce weight and drag. In a NASA study, the landing gear weight of a large TF cargo aircraft was 29.5% lighter than that of the reference conventional aircraft [63].

The aerostructural optimization results show that the SBW concept is more conducive to achieving a higher *AR* wing design for the MR mission studied in this work. Compared to the TF aircraft, the aerostructural optimization of the SBW aircraft increased the wing *AR* and at the same time reduced the wing mass more significantly. To realize the NLF wing design, the optimizers both reduced the wing sweep angle of the TF and SBW aircraft by adjusting wing airfoil shapes.

To provide a thorough basis for comparison and reference, we conducted a series of aerostructural optimizations in free transition mode on both the TF and SBW aircraft, applying conventional loading conditions of +2.5 g and -1.0 g to each, respectively. The comparison of the optimization results is given in Table 14, it is noteworthy that the Baseline TF and Baseline SBW in Table 14 were initially designed during the conceptual design phase, with load factors of +1.5 g and -0.5 g, respectively. The optimization results reveal that when subjected to conventional loading conditions, both the fuel weight and MTOW of the optimized TF and SBW aircraft exhibit substantial increases. These increases surpass the values obtained through optimization with reduced loading factors (i.e., +1.5 g/-0.5 g) and even exceed those of the baseline configurations. From Table 14, it can be seen that the optimizer both reduced the *AR* of the wing and increased the structural weight of the wing to cope with the higher wing loads. This increased both the aircraft structural weight and the aircraft fuel weight (due to decreased aerodynamic efficiency as well as increased MTOW). In addition, SBW achieves higher wing *AR* than TF for all load conditions

studied in this work, and the difference between the optimal AR of these two configurations is more significant for conventional loading conditions. Notably, in the case of the TF optimized under conventional loading conditions, an AR of 14.72 was achieved. This value closely aligns with the wing AR of the TF Stratolaunch carrier aircraft, which is approximately 14.9 [24].

**Table 13 Comparison of optimized configurations**

Parameter	A320neo [64]	Conceptual design		Aerostructural optimization	
		TF	SBW	TF	SBW
$m_F$ , kg	20980	12638	16117	10935	14406
MTOM, kg	79000	56155	67262	47758	61488
Empty mass, kg	44300	30229	37582	29374.5	34137
$m_W$ , kg	--	8101.8	11180.0	7247.3	7735
$m_{fuse}$ , kg	--	5241	7066	5241	7066
AR	10.5	24.33	25.81	20.74	26.01
$\Lambda$ , deg	25	9.70	10.54	7.80	8.88
$C_L$	--	0.3863	0.3893	0.3400	0.3778
$C_D$	--	0.0230	0.0229	0.0167	0.0175

**Table 14 Comparison of the TF and SBW aircraft under different loading conditions**

Configuration	$m_F$ , kg	MTOM, kg	$m_W$ , kg	AR
Baseline TF	12638	56155	8102	24.33
Opt. TF (+1.5 g/-0.5 g)	10935	47758	7247	20.74
Opt. TF (+2.5 g/-1.0 g)	14151	58441	10277	14.72
Baseline SBW	16117	67262	11180	25.81
Opt. SBW (+1.5 g/-0.5 g)	14406	61488	7735	26.01
Opt. SBW (+2.5 g/-1.0 g)	16824	73960	17438	25.62

## V. Conclusion

This study addressed the coupled adjoint aerostructural optimization problem of TF and SBW aircraft configurations with ultra-high aspect ratio wings. A mid-fidelity aerostructural optimization tool, which consisted of a geometrically nonlinear structural solver and a Q3D, NLF aerodynamic solver, was introduced and modified for the TF and SBW aircraft configurations. An aeroelastic and an aerostructural optimization were performed for an MR-TF and an MR-SBW aircraft, respectively.

In the aerostructural optimization, the wing planform, wing box structures, airfoil geometry, and the thickness-to-chord ratios of strut airfoils (only for SBW aircraft) were utilized as design variables. The optimization objective was to minimize the fuel mass while satisfying all the constraints on the wing (and strut, for SBW aircraft) structural failures, wing loading, and aileron effectiveness. The results showed more than a 10% reduction in fuel weight, more than 8% reduction in aircraft MTOM, and more than 30% reduction in wing and strut structural mass for the SBW aircraft; a more than 13% fuel weight

reduction, more than 14% MTOM reduction, and more than 10% wing structural mass reduction for the TF aircraft. In comparison to the original reference aircraft A320neo, the optimized TF and SBW have 48% and 31% lower fuel weight, respectively. The airfoil pressure coefficient distribution at different wing spanwise positions showed that the optimizer significantly reduced the compressibility drag of the wing and expanded the NLF range of both upper and lower wing surfaces.

The fuel mass and MTOM of the optimized TF aircraft are lighter than those of the SBW aircraft, which is mainly due to the better performance of the initial configuration (i.e., baseline configuration) of the TF aircraft. The aerostructural optimization results show that the SBW configuration is more conducive to realizing a higher aspect ratio wing design compared with the TF configuration for the medium-range mission studied in this paper.

This work preliminarily investigated the aerostructural optimization of the TF and SBW configurations. Avenues for future work include integrating flutter constraints into the aerostructural optimization and extending the aerostructural optimization for unconventional aircraft configurations to the high-fidelity level. In addition, this work focused on the TF and SBW aircraft for medium-range missions, while future studies can be extended to short- and long-range missions.

## References

- [1] "Airbus Global Market Forecast 2021 - 2040," Airbus, 2021.
- [2] "Commercial Market Outlook 2021-2040," Boeing, 2021.
- [3] European Commission, "Flightpath 2050: Europe's Vision for Aviation," Advisory Council for Aeronautics Research in Europe, Brussels, Belgium, 2011.
- [4] Beck, N., Landa, T., Seitz, A., Boermans, L., Liu, Y., and Radespiel, R., "Drag Reduction by Laminar Flow Control," *Energies*, Vol. 11, No. 1, 2018, p. 252.  
<https://doi.org/10.3390/en11010252>
- [5] Ma, Y., Karpuk, S., and Elham, A., "Conceptual Design and Comparative Study of Strut-Braced Wing and Twin-Fuselage Aircraft Configurations with Ultra-High Aspect Ratio Wings," *Aerospace Science and Technology*, Vol. 121, 2022, p. 107395.  
<https://doi.org/10.1016/j.ast.2022.107395>
- [6] Karpuk, S., and Elham, A., "Conceptual Design Trade Study for an Energy-Efficient Mid-Range Aircraft with Novel Technologies," presented at the AIAA Scitech 2021 Forum, VIRTUAL

- EVENT, 2021. <https://doi.org/10.2514/6.2021-0013>
- [7] Torenbeek, E., “Advanced Aircraft Design: Conceptual Design, Analysis, and Optimization of Subsonic Civil Airplanes,” Wiley, Chichester, 2013.
- [8] Chiesa, S., Di Sciuva, M., and Maggiore, P., “The Double-Fuselage Layout: A Preliminary Case Study of a Possible Way of Reducing the Development Costs for New High-Capacity Aircraft,” *Proceedings of the Institution of Mechanical Engineers, Part G: Journal of Aerospace Engineering*, Vol. 214, No. 2, 2000, pp. 85–95. <https://doi.org/10.1243/0954410001531836>
- [9] Vedernikov, Y. V., Chepiga, V. E., Maslakov, V. P., Kuklev, E. A., and Gusev, V. G., “Configuration of the Medium-Haul Twin-Fuselage Passenger Aircraft,” *International Journal of Applied Engineering Research*, Vol. 12, No. 4, 2017.
- [10] Gundlach, J. F., Tetrault, P.-A., Gern, F. H., Nagshineh-Pour, A. H., Ko, A., Schetz, J. A., Mason, W. H., Kapania, R. K., Mason, W. H., Grossman, B., and Haftka, R. T., “Conceptual Design Studies of a Strut-Braced Wing Transonic Transport,” *Journal of Aircraft*, Vol. 37, No. 6, 2000, pp. 976–983. <https://doi.org/10.2514/2.2724>
- [11] Gern, F., Ko, A., Grossman, B., Haftka, R., Kapania, R., Mason, W., and Schetz, J., “Transport Weight Reduction Through MDO: The Strut-Braced Wing Transonic Transport,” presented at the 35th AIAA Fluid Dynamics Conference and Exhibit, Toronto, Ontario, Canada, 2005. <https://doi.org/10.2514/6.2005-4667>
- [12] Hwang, J., Kenway, G., and Martins, J. R. R. A., “Geometry and Structural Modeling for High-Fidelity Aircraft Conceptual Design Optimization,” presented at the 15th AIAA/ISSMO Multidisciplinary Analysis and Optimization Conference, Atlanta, GA, 2014. <https://doi.org/10.2514/6.2014-2041>
- [13] Ricci, S., Paletta, N., Defoort, S., Benard, E., Cooper, J. E., and Barabinot, P., “U-HARWARD: A CS2 EU Funded Project Aiming at the Design of Ultra High Aspect Ratio Wings Aircraft,” presented at the AIAA SCITECH 2022 Forum, San Diego, CA & Virtual, 2022. <https://doi.org/10.2514/6.2022-0168>
- [14] Forte, C. J., Nguyen, N. T., and Xiong, J., “Gust Load Alleviation Control and Gust Estimation for a High Aspect Ratio Wing Wind Tunnel Model,” presented at the AIAA SCITECH 2023 Forum, National Harbor, MD & Online, 2023. <https://doi.org/10.2514/6.2023-0881>
- [15] Reddy, J. N., “Mechanics of Laminated Composite Plates and Shells: Theory and Analysis,” 2003.

- [16] Hosseini, S., Ali Vaziri-Zanjani, M., and Reza Ovesy, H., "Conceptual Design and Analysis of an Affordable Truss-Braced Wing Regional Jet Aircraft," *Proceedings of the Institution of Mechanical Engineers, Part G: Journal of Aerospace Engineering*, 2020, p. 095441002092306. <https://doi.org/10.1177/0954410020923060>
- [17] Ciampa, P. D., Prakasha, P. S., Torrigiani, F., Walther, J.-N., Lefebvre, T., Bartoli, N., Timmermans, H., Della Vecchia, P., Stingo, L., Rajpal, D., Van Gent, I., La Rocca, G., Fioriti, M., Cerino, G., Maierl, R., Charbonnier, D., Jungo, A., Aigner, B., Anisimov, K., Mirzoyan, A., and Voskuijl, M., "Streamlining Cross-Organizational Aircraft Development: Results from the AGILE Project," presented at the AIAA Aviation 2019 Forum, Dallas, Texas, 2019. <https://doi.org/10.2514/6.2019-3454>
- [18] Bradley, M. K., K. Dorney, C., and Allen, T., "Subsonic Ultra Green Aircraft Research: Phase II – Volume I – Truss Braced Wing Design Exploration," NASA/CR–2015-218704/Volume I, April 2015.
- [19] Gur, O., Bhatia, M., Mason, W. H., Schetz, J. A., Kapania, R. K., and Nam, T., "Development of a Framework for Truss-Braced Wing Conceptual MDO," *Structural and Multidisciplinary Optimization*, Vol. 44, No. 2, 2011, pp. 277–298. <https://doi.org/10.1007/s00158-010-0612-9>
- [20] Secco, N. R., and Martins, J. R. R. A., "RANS-Based Aerodynamic Shape Optimization of a Strut-Braced Wing with Overset Meshes," *Journal of Aircraft*, Vol. 56, No. 1, 2019, pp. 217–227. <https://doi.org/10.2514/1.C034934>
- [21] Kallo, J., "DLR Leads HY4 Project for Four-Seater Fuel Cell Aircraft," *Fuel Cells Bulletin*, Vol. 2015, No. 11, 2015, p. 13. [https://doi.org/10.1016/S1464-2859\(15\)30362-X](https://doi.org/10.1016/S1464-2859(15)30362-X)
- [22] Ma, Y., Zhang, W., and Elham, A., "Multidisciplinary Design Optimization of Twin-Fuselage Aircraft with Boundary-Layer-Ingesting Distributed Propulsion," *Journal of Aircraft*, Vol. 59, No. 6, 2022, pp. 1588–1602. <https://doi.org/10.2514/1.C036559>
- [23] Ma, Y., Zhang, W., Zhang, Y., Zhang, X., and Zhong, Y., "Sizing Method and Sensitivity Analysis for Distributed Electric Propulsion Aircraft," *Journal of Aircraft*, Vol. 57, No. 4, 2020, pp. 730–741. <https://doi.org/10.2514/1.C035581>
- [24] Corda, S., Longo, C., and Krevor, Z., "Stratolaunch Air-Launched Hypersonic Testbed," presented at the 22nd AIAA International Space Planes and Hypersonics Systems and Technologies Conference, Orlando, FL, 2018. <https://doi.org/10.2514/6.2018-5257>

- [25] Chau, T., and Zingg, D. W., “Aerodynamic Design Optimization of a Transonic Strut-Braced-Wing Regional Aircraft,” *Journal of Aircraft*, Vol. 59, No. 1, 2022, pp. 253–271. <https://doi.org/10.2514/1.C036389>
- [26] Ivaldi, D., Secco, N. R., Chen, S., Hwang, J. T., and Martins, J. R. R. A., “Aerodynamic Shape Optimization of a Truss-Braced-Wing Aircraft,” presented at the 16th AIAA/ISSMO Multidisciplinary Analysis and Optimization Conference, Dallas, TX, 2015. <https://doi.org/10.2514/6.2015-3436>
- [27] Ma, Y., and Elham, A., “Twin-Fuselage Configuration for Improving Fuel Efficiency of Passenger Aircraft,” *Aerospace Science and Technology*, Vol. 118, 2021, p. 107000. <https://doi.org/10.1016/j.ast.2021.107000>
- [28] Khan, K. H., Mallik, W., Kapania, R. K., and Schetz, J. A., “Distributed Design Optimization of Large Aspect Ratio Wing Aircraft with Rapid Transonic Flutter Analysis in Linux,” presented at the AIAA Scitech 2021 Forum, VIRTUAL EVENT, 2021. <https://doi.org/10.2514/6.2021-1354>
- [29] Meadows, N. A., Schetz, J. A., Kapania, R. K., Bhatia, M., and Seber, G., “Multidisciplinary Design Optimization of Medium-Range Transonic Truss-Braced Wing Transport Aircraft,” *Journal of Aircraft*, Vol. 49, No. 6, 2012, pp. 1844–1856. <https://doi.org/10.2514/1.C031695>
- [30] Van Gent, I., Aigner, B., Beijer, B., and La Rocca, G., “A Critical Look at Design Automation Solutions for Collaborative MDO in the AGILE Paradigm,” presented at the 2018 Multidisciplinary Analysis and Optimization Conference, Atlanta, Georgia, 2018. <https://doi.org/10.2514/6.2018-3251>
- [31] Boozer, C. M., and Elham, A., “COUPLED ADJOINT AEROSTRUCTURAL OPTIMIZATION FRAMEWORK FOR PRELIMINARY AIRCRAFT DESIGN,” presented at the 31st Congress of the International Council of the Aeronautical Sciences, Belo Horizonte, Brazil, 2018.
- [32] Guo, J., Li, Y., Xu, M., An, X., and Li, G., “Aero-Structural Optimization of Supersonic Wing under Thermal Environment Using Adjoint-Based Optimization Algorithm,” *Structural and Multidisciplinary Optimization*, Vol. 64, No. 1, 2021, pp. 281–301. <https://doi.org/10.1007/s00158-021-02888-1>
- [33] Gray, A. C., and Martins, J. R., “Geometrically Nonlinear High-Fidelity Aerostructural Optimization for Highly Flexible Wings,” presented at the AIAA Scitech 2021 Forum, VIRTUAL EVENT, 2021. <https://doi.org/10.2514/6.2021-0283>

- [34] Martins, J. R. R. A., Kennedy, G., and Kenway, G. K., “High Aspect Ratio Wing Design: Optimal Aerostructural Tradeoffs for the Next Generation of Materials,” presented at the 52nd Aerospace Sciences Meeting, National Harbor, Maryland, 2014. <https://doi.org/10.2514/6.2014-0596>
- [35] Kassapoglou, C., “Design and Analysis of Composite Structures: With Applications to Aerospace Structures,” Wiley, Hoboken, NJ, 2013.
- [36] Yang, T., Chen, Y., Shi, Y., Hua, J., Qin, F., and Bai, J., “Stochastic Investigation on the Robustness of Laminar-Flow Wings for Flight Tests,” *AIAA Journal*, Vol. 60, No. 4, 2022, pp. 2266–2286. <https://doi.org/10.2514/1.J060842>
- [37] Xu, J., and Kroo, I., “Aircraft Design with Active Load Alleviation and Natural Laminar Flow,” *Journal of Aircraft*, Vol. 51, No. 5, 2014, pp. 1532–1545. <https://doi.org/10.2514/1.C032402>
- [38] Schrauf, G., “Status and Perspectives of Laminar Flow,” *The Aeronautical Journal*, Vol. 109, No. 1102, 2005, pp. 639–644. <https://doi.org/10.1017/S000192400000097X>
- [39] Han, Z.-H., Chen, J., Zhang, K.-S., Xu, Z.-M., Zhu, Z., and Song, W.-P., “Aerodynamic Shape Optimization of Natural-Laminar-Flow Wing Using Surrogate-Based Approach,” *AIAA Journal*, Vol. 56, No. 7, 2018, pp. 2579–2593. <https://doi.org/10.2514/1.J056661>
- [40] Ma, Y., Abouhamzeh, M., and Elham, A., “Geometrically Nonlinear Coupled Adjoint Aerostructural Optimization of Natural-Laminar-Flow Strut-Braced Wing,” *Journal of Aircraft*, 2022, pp. 1–20. <https://doi.org/10.2514/1.C036988>
- [41] Elham, A., and van Tooren, M. J. L., “Coupled Adjoint Aerostructural Wing Optimization Using Quasi-Three-Dimensional Aerodynamic Analysis,” *Structural and Multidisciplinary Optimization*, Vol. 54, No. 4, 2016, pp. 889–906. <https://doi.org/10.1007/s00158-016-1447-9>
- [42] Abouhamzeh, M., Ma, Y., and Elham, A., “A Geometrically Nonlinear Structural Model For Aerostructural Optimization of Ultra-High Aspect Ratio Composite Wings,” presented at the AIAA SCITECH 2022 Forum, San Diego, CA & Virtual, 2022. <https://doi.org/10.2514/6.2022-0724>
- [43] Elham, A., “Adjoint Quasi-Three-Dimensional Aerodynamic Solver for Multi-Fidelity Wing Aerodynamic Shape Optimization,” *Aerospace Science and Technology*, Vol. 41, 2015, pp. 241–249. <https://doi.org/10.1016/j.ast.2014.12.024>
- [44] Drela, M., “MSES: Multi-Element Airfoil Design/Analysis Software,” Ver. 3.07, Massachusetts Institute of Technology, 2007.

- [45] Youngren, H., “Multi-Point Design and Optimization of a Natural Laminar Flow Airfoil for a Mission Adaptive Compliant Wing,” presented at the 46th AIAA Aerospace Sciences Meeting and Exhibit, Reno, Nevada, 2008. <https://doi.org/10.2514/6.2008-293>
- [46] Lasauskas, E., “INFLUENCE OF TRANSITION LOCATION ON AIRFOIL DRAG,” *Aviation*, Vol. 9, No. 3, 2005, pp. 19–22. <https://doi.org/10.3846/16487788.2005.9635906>
- [47] Wu, M., Han, Z., Nie, H., Song, W., Clainche, S. L., and Ferrer, E., “A Transition Prediction Method for Flow over Airfoils Based on High-Order Dynamic Mode Decomposition,” *Chinese Journal of Aeronautics*, Vol. 32, No. 11, 2019, pp. 2408–2421. <https://doi.org/10.1016/j.cja.2019.03.020>
- [48] Elham, A., and van Tooren, M. J., “Tool for Preliminary Structural Sizing, Weight Estimation, and Aeroelastic Optimization of Lifting Surfaces\*,” *Proceedings of the Institution of Mechanical Engineers, Part G: Journal of Aerospace Engineering*, Vol. 230, No. 2, 2016, pp. 280–295. <https://doi.org/10.1177/0954410015591045>
- [49] Rump, S. M., “INTLAB — INTerval LABoratory,” *Developments in Reliable Computing*, 1999.
- [50] Roskam, J., “Airplane Design, Part I: Preliminary Sizing of Airplanes,” Design, Analysis and Research Corporation, Lawrence, Kansas, 1997.
- [51] Ma, Y., Minisci, E., and Elham, A., “INVESTIGATING THE INFLUENCE OF UNCERTAINTY IN NOVEL AIRFRAME TECHNOLOGIES ON REALIZING ULTRA-HIGH ASPECT RATIO WINGS,” presented at the AeroBest 2021, 2021.
- [52] Horst, P., Elham, A., and Radespiel, R., “REDUCTION OF AIRCRAFT DRAG, LOADS AND MASS FOR ENERGY TRANSITION IN AERONAUTICS,” presented at the Deutsche Gesellschaft für Luft-und Raumfahrt-Lilienthal-Oberth eV, 2021, Bonn, Germany, 2021.
- [53] Karpuk, S., Radespiel, R., and Elham, A., “Assessment of Future Airframe and Propulsion Technologies on Sustainability of Next-Generation Mid-Range Aircraft,” *Aerospace*, Vol. 9, No. 5, 2022, p. 279. <https://doi.org/10.3390/aerospace9050279>
- [54] Hart-Smith, L. J., “The Ten-Percent Rule for Preliminary Sizing of Fibrous Composite Structures,” *Weight Engineering*, Vol. 52, 1992, pp. 29–45.
- [55] Elham, A., La Rocca, G., and Van Tooren, M. J. L., “Development and Implementation of an Advanced, Design-Sensitive Method for Wing Weight Estimation,” *Aerospace Science and Technology*, Vol. 29, No. 1, 2013, pp. 100–113. <https://doi.org/10.1016/j.ast.2013.01.012>

- [56] Bazant, Z. P., "Shear Buckling of Sandwich, Fiber Composite and Lattice Columns, Bearings, and Helical Springs: Paradox Resolved," *Journal of Applied Mechanics*, Vol. 70, No. 1, 2003, pp. 75–83. <https://doi.org/10.1115/1.1509486>
- [57] Vo, T. P., and Lee, J., "Geometrically Nonlinear Theory of Thin-Walled Composite Box Beams Using Shear-Deformable Beam Theory," *International Journal of Mechanical Sciences*, Vol. 52, No. 1, 2010, pp. 65–74. <https://doi.org/10.1016/j.ijmecsci.2009.10.005>
- [58] Sadraey, M., "Aircraft Design: A Systems Engineering Approach, Chapter 12 Design of Control Surfaces," 2012.
- [59] Roskam, J., "Airplane Design Part V: Component Weight Estimation," Design, Analysis and Research Corporation, 1985.
- [60] Sudhi, A., Radespiel, R., and Badrya, C., "Design of Transonic Swept Wing for HLFC Application," presented at the AIAA AVIATION 2021 FORUM, VIRTUAL EVENT, 2021. <https://doi.org/10.2514/6.2021-2606>
- [61] "Annex 14 to the Convention on International Civil Aviation - Aerodromes - Volume I Aerodrome Design and Operations," INTERNATIONAL CIVIL AVIATION ORGANIZATION, Montreal, 2018.
- [62] Metkowski, L. P., and Maughmer, M., "Winglet and Strut Configuration Study for a Slotted, Natural-Laminar-Flow Strut-Braced Transport Aircraft," presented at the AIAA Scitech 2021 Forum, VIRTUAL EVENT, 2021. <https://doi.org/10.2514/6.2021-0843>
- [63] Moore, J., and Maddalon, D., "Multibody Transport Concept," presented at the 2nd International Very Large Vehicles Conference, Washington,DC,U.S.A., 1982. <https://doi.org/10.2514/6.1982-810>
- [64] "A320 AIRCRAFT CHARACTERISTICS AIRPORT AND MAINTENANCE PLANNING," AIRBUS S.A.S., 31707 Blagnac Cedex FRANCE, 2020.